Identification of a divergent cytochrome *c* oxidase complex in the mitochondrial proteome of *Toxoplasma gondii*.

Azadeh Seidi[1,4,5], Linden S. Muellner-Wong[1,4,6], Esther Rajendran[1], Edwin T. Tjhin[1], Laura F. Dagley[2,3], Y.T. Vincent Aw[1], Andrew I. Webb[2,3], Christopher J. Tonkin[2,3], Giel G. van Dooren[1]

[1] Research School of Biology, Australian National University, Canberra, ACT, 2601, Australia

[2] The Walter and Eliza Hall Institute of Medical Research, 1G Royal Parade, Parkville, Victoria, 3052, Australia

[3] Department of Medical Biology, University of Melbourne, Parkville, Victoria, 3010, Australia

[4] Contributed equally

[5] current address: Australian Genome Research Facility, The Walter and Eliza Hall Institute of Medical Research, 1G Royal Parade, Parkville, Victoria, 3050, Australia

[6] current address: Department of Biochemistry and Molecular Biology, Monash Biomedicine Discovery Institute, Monash University, Melbourne, 3800, Australia

Address correspondence to Giel G. van Dooren, giel.vandooren@anu.edu.au

Keywords: *Toxoplasma*, mitochondria, apicomplexans, proteomics

ABSTRACT

The mitochondrion of apicomplexan parasites is critical for parasite survival, although the full complement of proteins that localize to this organelle has not been defined. Here we undertake two independent approaches to elucidate the mitochondrial proteome of the apicomplexan *Toxoplasma gondii*. We identify 421 mitochondrial proteins, many of which lack homologs in the animals that these parasites infect, and most of which are important for parasite growth. We demonstrate that one such protein, termed *Tg*ApiCox25, is an important component of the parasite cytochrome *c* oxidase (COX) complex. We identify numerous other apicomplexan-specific components of COX, and conclude that apicomplexan COX, and apicomplexan mitochondria more generally, differ substantially in their protein composition from the hosts they infect. Our study highlights the diversity that exists in mitochondrial proteomes across the eukaryotic domain of life, and provides a foundation for defining unique aspects of mitochondrial biology in an important phylum of parasites.

INTRODUCTION

Mitochondria were derived from α-proteobacteria in an endosymbiotic event, and were present in the last common ancestor of all eukaryotes (Gray, 2012; Sagan, 1967). Mitochondria and related organelles are present in almost all extant eukaryotes. They function in the biosynthesis of molecules such as iron-sulfur clusters, lipids, coenzyme Q, heme and amino acids, the catabolism of molecules such as fatty acids, amino acids and monocarboxylates, the storage of ions and signalling molecules such as Ca^{2+}, the regulation of apoptosis, and the production of energy-carrying molecules such as ATP and NADH (McBride et al., 2006; van Dooren et al., 2006; Zikova et al., 2016). Notably, the function of mitochondria and related organelles vary substantially between different eukaryotic lineages, reflective of the >1,500 M years that separate these lineages (Chernikova et al., 2011; Zikova et al., 2016).

Apicomplexans are a phylum of intracellular parasites that impose a significant medical and economic burden on human populations around the world. Apicomplexans include the causative agents of malaria (*Plasmodium* spp.), cryptosporidiosis (*Cryptosporidium* spp.) and toxoplasmosis (*Toxoplasma gondii*). *T. gondii* is an opportunistic parasite that chronically infects approximately one-third of the world's adult population. Symptoms of *T. gondii* infection in healthy individuals are typically mild. In immunocompromised individuals and unborn fetuses, however, *T. gondii* infection can cause severe neurological and developmental impairment, and, without treatment, can lead to death of the infected individual (Montoya and Liesenfeld, 2004). The tractable genetics of *T. gondii* make it a versatile model for studying conserved aspects of apicomplexan biology.

Mitochondria are critical for the survival of apicomplexans, and several important drugs target proteins that function in this organelle, including atovaquone and endochin-like quinolones, both

of which target cytochrome *c* reductase (complex III) of the electron transport chain, and DSM1, which targets dihydroorotate dehydrogenase, a central enzyme in pyrimidine biosynthesis (Doggett et al., 2012; Phillips et al., 2008; Srivastava et al., 1999). The functions of apicomplexan mitochondria are largely implied through comparative genomic approaches that have identified homologs of genes encoding known mitochondrial proteins from other eukaryotes (Seeber et al., 2008; van Dooren et al., 2006). The genome of apicomplexans such as *T. gondii* and *Plasmodium* spp. encode homologs of proteins involved in core mitochondrial processes such as the electron transport chain, the tricarboxylic acid (TCA) cycle, and the synthesis of molecules such as iron-sulfur clusters, heme and coenzyme Q (Seeber et al., 2008; van Dooren et al., 2006). The mitosome of *Cryptosporidium parvum* is highly reduced compared to that of other apicomplexans, lacking a TCA cycle, and harboring a minimal electron transport chain, but retaining the capacity for iron-sulfur cluster synthesis (Mogi and Kita, 2009).

Apicomplexans belong to a group of eukaryotes known as the myzozoans, that also include dinoflagellates and chromerids (Cavalier-Smith and Chao, 2004). Chromerids are a phylum of free-living, photosynthetic eukaryotes, and are thought to be the closest extant relatives of apicomplexans (Moore et al., 2008). All known myzozoans retain a mitochondrion or mitochondrion-derived organelle, the functions of which have numerous differences from well-studied eukaryotes such as yeast and animals (Danne et al., 2013; Jacot et al., 2015). In addition to a limited gene content, the mitochondrial genomes of these organisms contain unusually fragmented ribosomal RNAs (Feagin et al., 2012). Myzozoan mitochondria lack pyruvate dehydrogenase, the enzyme complex that decarboxylates pyruvate to form acetyl-CoA (Danne et al., 2013; Foth et al., 2005). Instead, these organisms have repurposed a branched-chain α-ketoacid dehydrogenase (BCKDH) to catalyse this reaction (Oppenheim et al., 2014).

Myzozoans have a functional TCA cycle, but some enzymes of this pathway are phylogenetically distinct from equivalent enzymes in yeast and humans (Danne et al., 2013; Ke et al., 2015; MacRae et al., 2013; MacRae et al., 2012; van Dooren et al., 2006). These organisms also contain a mitochondrial ATP synthase that lacks clear homologs to many of the proteins that comprise the membrane-bound F_0 component of the complex (Balabaskaran Nina et al., 2011; Sturm et al., 2015).

Elucidating the proteomes of mitochondria is key to understanding their functions. Organellar proteomics in intracellular parasites such as *T. gondii* is limited by available material and a lack of established organellar purification techniques. To overcome these obstacles, we adopted two complementary spatially-restricted biotin tagging approaches to define the proteome of the mitochondrial matrix of *T. gondii*. We identified over 400 putative mitochondrial matrix proteins, many of which have no ascribed function and no clear homology to proteins found in well-characterised eukaryotes such as yeast, and most of which are important for parasite growth and survival. We functionally characterise one protein that had no previously ascribed function, and demonstrate that this is a critical component of the cytochrome *c* oxidase (COX) complex of the mitochondrial electron transport chain in the parasite. We subsequently identify numerous apicomplexan-specific components of COX. These data reveal considerable divergence in the COX complex, and in mitochondria more generally, of *T. gondii* and related apicomplexans, compared to the animals they infect.

RESULTS

Spatially-restricted biotinylation of mitochondrial matrix proteins. A genetically modified plant ascorbate peroxidase (APEX) was recently developed as a tool for biotinylating proximal proteins in mammalian cells (Hung et al., 2014; Rhee et al., 2013). This technique was used to define the proteome of the matrix and inter-membrane space of mammalian mitochondria. An alternative spatial biotinylation approach involves the use of a genetically modified, promiscuous biotin protein ligase (BirA*), an approach that is typically utilised to elucidate protein-protein interactions (Roux et al., 2012). We sought to utilize APEX and BirA* to map the mitochondrial matrix proteome of *T. gondii*.

We generated parasite strains expressing APEX or BirA* fused at their N-termini to the mitochondrial matrix-targeting sequence of *Tg*Hsp60 (van Dooren et al., 2009). Immunofluorescence assays demonstrated that both mitochondrially-targeted APEX (mtAPEX) and mitochondrially-targeted BirA* (mtBirA*) co-localised with *Tg*Tom40, a marker for the *T. gondii* mitochondrion (Figure 1A-B; (van Dooren et al., 2016)). Western blots confirmed the presence of mtAPEX and mtBirA* proteins of the expected mass (Figure 1C-D).

To determine whether mtAPEX could label mitochondrial proteins, we treated parasites with biotin-phenol for 1 hr, initiated biotinylation by adding H_2O_2 for 1 min, then fixed and labelled parasites with Oregon green-conjugated avidin, a specific stain for biotinylated proteins. We observed mitochondrial labelling in treated parasites, and not in untreated parasites (Figure 1E), consistent with mtAPEX mediating the biotinylation of mitochondrial proteins. In untreated parasites, we observed labelling of endogenously biotinylated proteins in the apicoplast, consistent with previous observations (Figure 1E; (Chen et al., 2015; Jelenska et al., 2001)).

To determine whether mtBirA* could label mitochondrial proteins, we incubated mtBirA*-expressing parasites in medium supplemented with 1 mM biotin for 1 day. We labelled parasites with Oregon green-conjugated avidin and observed labelling in the mitochondrion of biotin-supplemented parasites, but not in untreated parasites (Figure 1F).

To observe the extent of protein biotinylation in the treated mtAPEX and mtBirA* parasites, we extracted proteins from RH strain wild type (WT), mtAPEX or mtBirA* parasites treated with either biotin-phenol and H_2O_2 or with biotin. We separated these by SDS-PAGE and probed with horse radish peroxidase (HRP)-conjugated neutravidin to label biotinylated proteins. In WT cells, we observed two major bands of the expected sizes of natively biotinylated proteins in these parasites (Figure 1G; (van Dooren et al., 2008)). In the biotin-phenol treated mtAPEX parasites, we observed labelling of several additional proteins, whereas in biotin-supplemented mtBirA* parasites, numerous proteins were labelled (Figure 1G). These data indicate that mtAPEX- and mtBirA*-mediated biotinylation is occurring in these parasites.

To determine the specificity of labelling, we extracted proteins from treated WT, mtAPEX and mtBirA* parasites and subjected these to affinity purification using streptavidin-conjugated magnetic beads. We separated purified proteins by SDS-PAGE and probed with antibodies against *Tg*Hsp60 (mtHsp60), a mitochondrial matrix marker (Toursel et al., 2000; van Dooren et al., 2016), and against *T. gondii* cytochrome *c* (cyt *c*), a mitochondrial intermembrane space marker (E.T. and G.v.D., unpublished). We did not detect mtHsp60 or cyt *c* in the streptavidin bound fraction in WT parasites treated with biotin-phenol and H_2O_2, or with biotin (Figure 1H).

We detected bound mtHsp60, but not bound cyt *c*, in proteins extracted from both biotin-phenol-treated mtAPEX and biotin-treated mtBirA* parasites. This is consistent with the mitochondrial labelling that we observe being specific for the mitochondrial matrix.

Quantitative proteomics to elucidate the mitochondrial matrix proteome. Having established two independent approaches for specifically labelling mitochondrial matrix proteins, we next undertook a label-free quantitative proteomic analysis of biotinylated proteins in treated mtAPEX and mtBirA* parasites. First, we generated 3 independent cell lysate pools of WT and mtAPEX cells treated with biotin-phenol and H_2O_2, and WT and mtBirA* cells treated with biotin. Biotinylated proteins were purified from these lysates using streptavidin beads, reduced, alkylated, and trypsin-digested before being identified using mass spectrometry (MS). Triplicate samples were then processed through our in-house quantitation pipeline to determine the relative abundance of each protein identified in the mtAPEX or mtBirA* samples as compared to WT controls. These data are represented on a volcano plot as a fold-change ($\log_2$ value) vs significance of the change ($-\log_{10} p$ value) (Figure 2A-B). This revealed an enrichment of numerous proteins in the mtAPEX and mtBirA* samples. Using cut-offs of $p < 0.001$ and a WT:mtAPEX/mtBirA* $\log_2$ fold change of <-2.5, 421 proteins were identified in total: 213 proteins in the APEX samples and 369 proteins in the mtBirA* samples, with 161 proteins common to both proteomes (Figure 2C; Supplementary File 1). Hereafter, we refer to the list of 421 proteins as the mitochondrial proteome of *T. gondii*.

Bioinformatic characterisation of the mitochondrial proteome. To test the validity of the *T. gondii* mitochondrial proteome, we undertook a series of *in silico* and experimental analyses.

Proteins targeted to the mitochondrial matrix typically harbor an N-terminal amphipathic α-helix that facilitates import into the organelle (van Dooren et al., 2016). We examined the *T. gondii* mitochondrial proteome for proteins predicted to contain such an N-terminal targeting domain using the rules-based computational prediction tool MitoProt II (Claros and Vincens, 1996). Approximately 40% of proteins in the proteome had a strongly predicted N-terminal targeting sequences (probability of mitochondrial import >0.9), and a further ~20% had a moderately predicted targeting sequence (probability of import 0.5 - 0.9; Figure 2 – figure supplement 1; Supplementary File 1). A further ~40% had a low probability of mitochondrial import (probability of import <0.5; Figure 2 – figure supplement 1). This suggests that either the mitochondrial proteome has many false positives, or that many *T. gondii* mitochondrial proteins lack N-terminal targeting sequences, or that mitochondrial prediction tools such as MitoProt II are not suitable for analysis of mitochondrial proteins from *T. gondii*. Notably in this regard, the dataset used to develop MitoProt II did not include *T. gondii* proteins (Claros and Vincens, 1996).

Next, we examined metabolic pathway enrichment of the mitochondrial proteome (http://toxodb.org; (Gajria et al., 2008); *p* value cutoff <0.05; Supplementary File 2). We observed the greatest enrichment in proteins involved in the TCA cycle, oxidative phosphorylation, and pyruvate metabolism, all processes predicted to occur in the mitochondrion. We observed enrichment of other processes predicted to occur in the mitochondrion, including ubiquinone biosynthesis, one carbon metabolism, and branched chain amino acid degradation. We also observed enrichment of some processes not expected to occur

in the mitochondrion, such as glycolysis/gluconeogenesis, suggesting the presence of some false positives in our proteome.

To analyse the mitochondrial proteome in greater detail, we mapped proteins to previously constructed metabolic maps of apicomplexan mitochondria (Supplementary File 3; (Seeber et al., 2008; van Dooren et al., 2006)). This analysis identified all subunits of the BCKDH, all enzymes of the TCA cycle, all proteins predicted to function in mitochondrial Fe-S cluster synthesis, four of the seven enzymes predicted to function in coenzyme Q synthesis, and two of the three mitochondrial proteins involved in heme synthesis (Figure 2D). Additionally, we identified all five ubiquinone-reducing dehydrogenases of the mitochondrial inner membrane, and all currently predicted subunits of cytochrome *c* reductase (Complex III) and cytochrome *c* oxidase (Complex IV) that are encoded on the nuclear genome (Figure 2D). We were unable to identify cytochrome *b*, CoxI and CoxIII, proteins encoded on the mitochondrial genome apicomplexan parasites. As expected, we did not identify the two isoforms of cytochrome *c*, both predicted to localize to the intermembrane space. We identified the α, β, γ and δ subunits of the F_1 component of ATP synthase, but not the ε subunit.

We identified numerous other proteins shown previously to localise to the mitochondrion (Supplementary File 3), including components of the presequence translocase associated motor (van Dooren et al., 2016), the aforementioned *Tg*Hsp60 (Toursel et al., 2000), components of the mitochondrial processing peptidase (van Dooren et al., 2016), a mitochondrial pyruvate kinase (Saito et al., 2008), a component of the γ–aminobutyric acid shunt (MacRae et al., 2012), an enzyme involved in phospholipid synthesis (Hartmann et al., 2014), and proteins associated with

DNA repair (Garrison and Arrizabalaga, 2009) and antioxidant defences (Brydges and Carruthers, 2003; Ding et al., 2004). Notably, we were unable to identify mitochondrially-localised enzymes involved in the 2-methylcitrate cycle (Limenitakis et al., 2013). We identified several conserved solute transporter proteins, and numerous proteins with housekeeping roles in the mitochondrion, including mitochondrial RNA polymerase, 18 ribosomal proteins (Gupta et al., 2014), ribosome maturation factors, and various translation elongation factors (Supplementary File 3). A recent genome-wide CRISPR-based screen to identify genes important for *in vitro* growth of tachyzoite-stage *T. gondii* identified 15 so-called Indispensable Conserved Apicomplexan Proteins (ICAPs; (Sidik et al., 2016)). Of these, 8 localised to the mitochondrion. We identified 6 of these mitochondrial ICAPs in the mitochondrial proteome. In total, our proteomics identified 96 out of 110 proteins that previously studies had experimentally localized, or predicted to localize, to the mitochondrion, suggesting a high level of coverage (87%).

We examined the mitochondrial proteome for likely false positives. We identified 17 proteins that other studies have demonstrated do not localise to the mitochondrion (Supplementary File 3). Notably, 15 of these were identified only in the mtBirA* proteome, while 2 were present in both the mtBirA* and mtAPEX proteomes. In total, of the 421 proteins in the mitochondrial proteome, we identified 96 (23%) that are known or expected to localise to the mitochondrion, and 17 (4%) that are known to localise elsewhere.

Localisation of uncharacterized proteins from the mitochondrial proteome. Of the 421 putative mitochondrial proteins identified in the mitochondrial proteome, 150 (36%) were annotated as

241 'hypothetical' proteins, and a further 140 (33%) had no previously defined role or experimentally
242 determined localization in *T. gondii* (Supplementary File 1). We attempted to localize 37
243 proteins selected at random from this 'uncharacterized' protein data set by introducing a
244 hemagglutinin (HA) epitope tag at the 3' end of the native locus of genes encoding these
245 proteins. We then undertook immunofluorescence assays to determine the localization of the
246 proteins, co-labelling with anti-*Tg*Tom40 as a marker for the mitochondrion (van Dooren et al.,
247 2016). We were successful in localizing 27 of the 37 selected proteins. Of these, 22 (81%)
248 localized to the mitochondrion, three to the cytosol, one to the endoplasmic reticulum and one to
249 the nucleus (Figure 3). All 13 that were identified in both the mtAPEX and mtBirA* proteomes
250 localized to the mitochondrion, suggesting a high degree of confidence in the mitochondrial
251 localization of proteins identified from both datasets. Five of the six proteins found solely in the
252 mtAPEX proteome localized to the mitochondrion, while four of the eight proteins found only in
253 the mtBirA* proteome localized to the mitochondrion.
254
255 ***Phylogenetic analyses of the mitochondrial proteome.*** We next examined the evolutionary
256 history of proteins from the mitochondrial proteome. First, we undertook reciprocal Basic Local
257 Alignment Search Tool (BLAST) searches to identify homologs of proteins from the
258 mitochondrial proteome in the apicomplexan parasites *Plasmodium falciparum*, *Babesia bovis*
259 and *Cryptosporidium parvum*, and the chromerid *Vitrella brassicaformis*. Using this approach,
260 we identified homologs for 71% of *T. gondii* mitochondrial proteins in *P. falciparum*, 61% in *B.*
261 *bovis*, 28% in *C. parvum,* and 83% in *V. brassicaformis* (Figure 4A).
262

263 We were next interested in the extent of novelty in the *T. gondii* mitochondrial proteome when
264 compared to non-apicomplexan eukaryotes. We examined conserved orthology groupings of the
265 421 proteins in the mitochondrial proteome and identified 418 proteins that clustered into 412
266 separate orthology groups (http://orthomcl.org; (Chen et al., 2006)). We identified 86 proteins
267 that were unique to *T. gondii* and closely related coccidians such as *Neospora caninum*, 243
268 proteins with orthologs in non-apicomplexan eukaryotes, and a set of 89 proteins that were found
269 only in apicomplexans and/or chromerids (Figure 4B; Supplementary File 1).
270
271 Novel drug targets against apicomplexans are likely to emerge from proteins which lack
272 homologs in animals. We therefore conducted an orthology analysis comparing the *T. gondii*
273 mitochondrial proteome to other apicomplexans, chromerids and animals. We found that 51% of
274 the mitochondrial proteome lacked orthologs in animals, of which 56% had orthologs in other
275 apicomplexans and/or chromerids (Figure 4C). The remainder were restricted to *T. gondii* and
276 other coccidian parasites such as *N. caninum*.
277
278 ***Phenotype analyses of the mitochondrial proteome.*** Our data indicate substantial novelty in
279 mitochondrial biology of *T. gondii* and related organisms. Often, such derived features are less
280 important for an organism's survival than proteins that have been conserved across evolution. A
281 recent genome-wide, CRISPR-based loss-of-function screen in *T. gondii* found that genes
282 conserved in eukaryotes were, in general, more important for parasite fitness than genes with a
283 more restricted phylogenetic distribution (Sidik et al., 2016). To determine whether the same was
284 true for mitochondrial proteins, we analysed the *T. gondii* mitochondrial proteome using the
285 Sidik et al data set (Sidik et al., 2016). The Sidik et al study ascribed phenotype scores to each

gene in the *T. gondii* nuclear genome, with more negative scores indicative of a greater importance for a gene's contribution to parasite fitness. The Sidik et al study found that most genes that were important for parasite growth had phenotype scores of below -2, and most dispensable genes had phenotype scores of greater than -2 (Sidik et al., 2016). Based on this, we categorised proteins in the mitochondrial proteome as dispensable (phenotype score >-2), important (-2 to -4), or critical (<-4) for parasite growth. Notably, 35% of proteins from the mitochondrial proteome were critical, and 39% were important, for parasite growth (Figure 4A; Supplementary File 1). Of the *T. gondii* mitochondrial proteins with orthologs in *P. falciparum*, ~75% were important or critical, and similar values apply for those with orthologs in *B. bovis*, *C. parvum*, and *V. brassicaformis* (Figure 4A). Of the proteins conserved between *T. gondii* and apicomplexans/chromerids, over 80% were important or critical for parasite growth, while over 70% of proteins collectively found in apicomplexans, chromerids and animals were important or critical (Figure 4D; Supplementary File 1).

***Tg*ApiCox25 is important for mitochondrial oxygen consumption in *T. gondii*.** Having identified ~175 proteins in the *T. gondii* mitochondrial proteome that have no clear orthologs outside the apicomplexan/chromerid lineage, and no predicted function, we embarked on a broad project to characterise the importance and role of these proteins. In the remainder of this manuscript, we focus on one such protein, annotated as TGGT1_264040, which (for reasons that will become apparent) we termed *Tg*ApiCox25. *Tg*ApiCox25 belongs to an OrthoMCL ortholog grouping that is restricted to apicomplexans, contains no recognisable functional domains, and is important for parasite fitness. It has a predicted molecular mass of 25 kDa, and we confirmed its localisation to the mitochondrion (Figure 3R). To establish the importance of *Tg*ApiCox25 for

parasite growth, and to facilitate subsequent characterisation of its function, we replaced the native promoter of *Tg*ApiCox25 with an anhydrotetracycline (ATc)-regulated promoter using a CRISPR-based genome editing approach (Figure 5 – figure supplement 1A). We performed PCR screening analysis to identify clonal parasites that had integrated the ATc-regulated promoter into the *Tg*ApiCox25 locus (Figure 5 – figure supplement 1B-C). We termed the resultant ATc-regulated *Tg*ApiCox25 strain 'r*Tg*ApiCox25'. We then introduced a HA tag at the 3' end of the open reading frame of the r*Tg*ApiCox25 locus. We termed the resultant HA-tagged, ATc-regulated *Tg*ApiCox25 strain 'r*Tg*ApiCox25-HA'. To measure the extent of target protein knockdown upon the addition of ATc in the r*Tg*ApiCox25 strain, we cultured parasites in the absence of ATc, or in the presence of ATc for 1-3 days, then undertook western blotting. This revealed substantial depletion of *Tg*ApiCox25-HA 2 days after ATc addition, with the *Tg*ApiCox25-HA protein barely detectable after 3 days in ATc (Figure 5A). To determine the importance of *Tg*ApiCox25 on parasite growth we compared plaque sizes of parental wild type (WT) and r*Tg*ApiCox25 parasites grown in the absence or presence of ATc for 9 days. This revealed that growth of r*Tg*ApiCox25, but not WT, parasites was severely impaired in the presence of ATc (Figure 5B-C). Interestingly, r*Tg*ApiCox25 parasites grew better in the absence of ATc than WT parasites (Figure 5B-C). To determine whether the growth phenotype observed upon *Tg*ApiCox25 knockdown was specifically due to loss of *Tg*ApiCox25, we complemented the r*Tg*ApiCox25 strain with a constitutive copy of *Tg*ApiCox25 (generating a strain we termed c*Tg*ApiCox25-HA/r*Tg*ApiCox25). The presence of the constitutive copy of *Tg*ApiCox25 restored growth of r*Tg*ApiCox25 parasites in the presence of ATc (Figure 5B-C).

A major function of the mitochondrion is in oxidative phosphorylation, where the catabolism of organic molecules by the TCA cycle and other metabolic pathways contribute electrons to an electron transport chain on the inner membrane of the organelle (van Dooren et al., 2006). Electrons are ultimately used to reduce O_2, with the electron transport chain simultaneously generating a proton gradient across the inner membrane. This proton gradient is then used to drive the F-type ATP synthase, a rotary motor that phosphorylates ADP to form ATP, the energy currency of cells. Defects in any of the processes involved in oxidative phosphorylation will lead to defects in mitochondrial O_2 consumption. To test whether *Tg*ApiCox25 has a role in oxidative phosphorylation, we established an assay to measure O_2 consumption by the parasite using a Seahorse XFe96 extracellular flux analyzer. We grew r*Tg*ApiCox25 parasites in the absence of ATc, or presence of ATc for 1-3 days then used the XFe96 analyzer to measure basal mitochondrial O_2 consumption rates (mOCR) in extracellular parasites. This revealed a significant, ~80% depletion in basal mOCR upon *Tg*ApiCox25 knockdown (Figure 5D), concomitant with knockdown of protein levels (Figure 5A).

Treatment with the protonophore FCCP uncouples OCR from ATP synthesis and enables the determination of maximal mOCR in parasites. We found that maximal mOCR was also depleted upon *Tg*ApiCox25 knockdown (Figure 5 – figure supplement 2). In a concomitant study, we demonstrated that depletion of a component of *T. gondii* ATP synthase led to an increase in the spare capacity of mOCR (i.e. the difference between the basal and maximal mOCR; see accompanying manuscript by Huet et al). We did not observe an increase in spare capacity upon *Tg*ApiCox25 knockdown (Figure 5 – figure supplement 2), indicating that *Tg*ApiCox25 is not a component of ATP synthase. Basal and maximal mOCR in WT parasites were unaffected by the

addition of ATc, although, curiously, the spare capacity in WT parasites was greater than in r*Tg*ApiCox25 parasites grown in the absence of ATc (Figure 5 – figure supplement 2). This is perhaps reflective of changes in *Tg*ApiCox25 protein abundance or timing of expression upon replacing the native promoter with the ATc-regulated promoter.

We wondered whether the defect in mOCR upon *Tg*ApiCox25 knockdown was the result of general defects in mitochondrial function or parasite viability. To address this, we first measured the extracellular acidification rate (ECAR) in WT and r*Tg*ApiCox25 parasites grown in the absence or presence of ATc. ECAR is measured simultaneously with OCR by the XFe96 analyzer. In mammalian cells, ECAR is thought to depend on the extrusion of lactate, and is therefore a measure of glycolysis (Ferrick et al., 2008). The contribution of glycolysis and other processes that acidify the extracellular medium (e.g. activity of the plasma membrane proton pump of these parasites; (Moreno et al., 1998)) to ECAR in *T. gondii* are not yet understood. Nevertheless, we can use ECAR measurements as a general indication of parasite metabolic activity. ECAR levels in WT parasites was approximately 40 mpH/min/1.5 x 10^6 parasites, and slightly less in r*Tg*ApiCox25 parasite grown the absence of ATc. Growth of *Tg*ApiCox25 parasites for 2 or 3 days in ATc resulted in a slight increase in ECAR (Figure 5E), indicating that parasites remained metabolically active upon *Tg*ApiCox25 knockdown. As a control for non-metabolically active parasites, we treated WT parasites with the translation inhibitor cycloheximide for 24 hr, which would be expected to deplete key metabolic enzymes in the parasite. XFe96 measurements revealed that both mOCR and ECAR were depleted upon cycloheximde treatment (Figure 5E), consistent with a general loss of parasite metabolism

leading to simultaneous defects in mOCR and ECAR. We conclude that parasites remain metabolically active in the absence of *Tg*ApiCox25.

Next, we asked whether knockdown of *Tg*ApiCox25 led to general defects in mitochondrial morphology. We performed immunofluorescence assays labelling the mitochondrion in r*Tg*ApiCox25 parasites grown in the absence or presence of ATc. This revealed no gross morphological defects in mitochondrial morphology upon the loss of *Tg*ApiCox25 (Figure 5 – figure supplement 3A). Finally, we asked whether *T. gondii* parasites remained viable upon knockdown of *Tg*ApiCox25. We pre-incubated r*Tg*ApiCox25 parasites in the presence of ATc for 3 days. We then set up plaque assays in the absence or presence of ATc, comparing parasite growth with parasites that had not been pre-incubated in ATc. As expected, parasites that were maintained in ATc for the duration of the plaque assay underwent minimal growth, regardless of whether they were pre-incubated in ATc (Figure 5 – figure supplement 3B). Notably, plaque number and size were equivalent between pre-incubated and non-pre-incubated parasites when grown in the absence of ATc. This reveals that *Tg*ApiCox25 knockdown is reversible and, importantly, that r*Tg*ApiCox25 parasites treated for 3 days on ATc have equivalent viability to r*Tg*ApiCox25 not grown on ATc.

The data presented here indicate that the defects we observed in mitochondrial O_2 consumption upon *Tg*ApiCox25 knockdown are not due to general defects in parasite viability, metabolism or mitochondrial morphology. We conclude that *Tg*ApiCox25 has an important, specific role in oxidative phosphorylation in *T. gondii* parasites.

399 ***Tg*ApiCox25 is a component of cytochrome *c* oxidase.** Our findings that *Tg*ApiCox25 is
400 critical for mitochondrial O_2 consumption prompted us to investigate whether this protein is a
401 component of the mitochondrial electron transport chain that mediates O_2 consumption. The
402 mitochondrial electron transport chain consists of several large protein complexes. To determine
403 whether *Tg*ApiCox25 exists in a protein complex, we extracted proteins from *Tg*ApiCox25-HA
404 parasites using 1% (v/v) Triton X-100 detergent, and separated these proteins by blue native-
405 PAGE, a technique that preserves the native conformation of proteins and protein complexes.
406 Western blotting of *Tg*ApiCox25-HA extracts separated by blue native-PAGE and detected with
407 anti-HA antibodies revealed that *Tg*ApiCox25-HA exists at a molecular mass of ~600 kDa
408 (Figure 6A). By contrast, the monomeric form of *Tg*ApiCox25-HA, extracted from parasites and
409 separated by SDS-PAGE, had a mass of approximately 25 kDa (Figure 6B). We conclude that
410 *Tg*ApiCox25 is a component of a ~600 kDa protein complex in the parasite mitochondrion.
411
412 To elucidate the proteins that comprise the *Tg*ApiCox25-containing complex, we
413 immunoprecipitated *Tg*ApiCox25-HA and associated proteins with anti-HA-coupled agarose
414 beads (Figure 6 – figure supplement 1A), then performed mass spectrometry to identify the
415 proteins that were part of this complex. As a negative control, we immunopurified *Tg*Tom40-HA
416 (Figure 6 – figure supplement 1B), the central protein of the ~400 kDa translocon of the outer
417 mitochondrial membrane (TOM) complex (van Dooren et al., 2016), and subjected these extracts
418 to mass spectrometry-based protein identification. Using this approach, we identify 12 proteins,
419 including *Tg*ApiCox25, that were enriched in the *Tg*ApiCox25-HA immunoprecipitation
420 compared to the *Tg*Tom40-HA immunoprecipitation (Figure 6C; Table 1; Supplementary File 5).
421 Of these 12 proteins, three are annotated as being canonical components of cytochrome *c* oxidase

(COX, also known as Complex IV of the mitochondrial electron transport chain; Figure 6C; Table 1). These proteins included *Tg*Cox2A (TGGT_226590) and *Tg*Cox2b (TGGT1_310470), split Cox2 homologs that are found in apicomplexans and which have previously been localised to the mitochondrion of *T. gondii* (Funes et al., 2002; Morales-Sainz et al., 2008), as well as *Tg*Cox5b (TGGT1_209260). Profile hidden Markov model similarity searches revealed that 7 of the remaining 8 *Tg*ApiCox25-associated proteins have homologs in other apicomplexans as well as in chromerids, whereas one (TGGT1_265370; *Tg*ApiCox16) is restricted to *T. gondii* (Table 1). All of the proteins detected were identified in the mitochondrial proteome (Table 1; Supplementary File 1), including TGGT1_297810 (*Tg*ApiCox30), an HA-tagged version of which we previously confirmed localizes to the mitochondrion in immunofluorescence assays (Figure 3X). All these proteins except *Tg*ApiCox16 are predicted to be important for growth of the tachyzoite stage of *T. gondii* (Table 1; (Sidik et al., 2016)).

As a direct test for whether *Tg*ApiCox25 interacts with *Tg*Cox2a, we introduced a FLAG epitope tag into the native locus of *Tg*Cox2a in the *Tg*ApiCox25-HA background strain, generating a strain we termed *Tg*Cox2a-FLAG/*Tg*ApiCox25-HA (Figure 7 – figure supplement 1A-B). We separated proteins from the *Tg*Cox2a-FLAG/*Tg*ApiCox25-HA strain using blue native-PAGE and performed western blotting with anti-FLAG antibodies. This revealed that *Tg*Cox2a-FLAG exists in a protein complex of ~600 kDa (Figure 7A). Immunoprecipitation of *Tg*Cox25-HA with anti-HA antibodies co-purified *Tg*Cox2a-FLAG, but not *Tg*AtpB, the β–subunit of the F_1 domain of ATP synthase, or the mitochondrial outer membrane protein *Tg*Tom40 (Figure 7B)). Similarly, immunoprecipitation of *Tg*Cox2a-FLAG with anti-FLAG antibodies co-purified

444 *Tg*ApiCox25, but not *Tg*AtpB or *Tg*Tom40 (Figure 7B). Together, these data indicate that
445 *Tg*Cox2a-FLAG exists in the same complex as *Tg*ApiCox25-HA.
446
447 To test whether *Tg*ApiCox25 interacts with *Tg*ApiCox30, we introduced a FLAG epitope tag
448 into the native locus of TgApiCox25 in the *Tg*ApiCox30-HA background, generating a strain we
449 termed *Tg*ApiCox25-FLAG/*Tg*ApiCox30-HA (Figure 7 – figure supplement 1C-D). Western
450 blots of proteins separated by blue native-PAGE indicated that both *Tg*ApiCox25-FLAG and
451 *Tg*ApiCox30-HA exist in a ~600 kDa protein complex (Figure 7C). Immunoprecipitation of
452 *Tg*ApiCox30 with anti-HA antibodies purified *Tg*ApiCox25 but not *Tg*AtpB or *Tg*Tom40, and
453 immunoprecipitation of *Tg*ApiCox25 with anti-FLAG antibodies co-purified *Tg*ApiCox30 but
454 not *Tg*AtpB or *Tg*Tom40 (Figure 7D). We conclude that *Tg*ApiCox25-FLAG and *Tg*ApiCox30-
455 HA exist in the same protein complex.
456
457 Combined with the observation that *Tg*ApiCox25 is important for mitochondrial O_2 consumption
458 (Figure 5D), these data are consistent with the hypothesis that *Tg*ApiCox25 and *Tg*ApiCox30 are
459 components of the parasite COX complex, the terminal oxidase of the mitochondrial electron
460 transport chain that facilitates the reduction of O_2. To reflect their apparent phylogenetic
461 restriction to apicomplexans and related organisms, we have termed the apicomplexan-specific
462 components of the *T. gondii* COX complex as "ApiCox" proteins, with the numerical suffix
463 indicating the predicted molecular mass of the protein (Table 1).
464
465 To investigate whether proteins from the *Tg*ApiCox25 complex might have structural similarity
466 to known proteins, we queried each protein enriched in the *Tg*ApiCox25 immunoprecipitation

against the Protein Data Bank (PDB) using HHPRED, a profile hidden Markov model search tool that also incorporates secondary structure information (Zimmermann et al., 2017). As expected, *Tg*Cox2a, *Tg*Cox2b and *Tg*Cox5b had homology to equivalent cytochrome *c* oxidase proteins from other eukaryotes (probability > 99%, e value < 5.1 e^{-16} for each). Interestingly, *Tg*ApiCox25 had predicted homology to cytochrome *c* oxidase complex subunit 6A from *Bos taurus* (PDB annotation 5B1A_T; probability 90.9%, e value 0.58) and *Tg*ApiCox23 had predicted homology to cytochrome *c* oxidase complex subunit 4 from *Bos taurus* (PDB annotation 5B1A_D; probability 95.57%, e value 0.0057). None of the remaining ApiCox proteins were matched to proteins from PDB with any great confidence (probability of homology to the top "hit" < 70%, e value > 5 for all).

To obtain insights into the role of *Tg*ApiCox25 in the parasite COX complex, we tested the effects of *Tg*ApiCox25 knockdown on complex integrity. We introduced a FLAG epitope tag into the *Tg*Cox2a locus of the r*Tg*ApiCox25-HA parasite strain, generating a strain we term *Tg*Cox2a-FLAG/r*Tg*ApiCox25-HA (Figure 7 – figure supplement 1A-B). We grew parasites in the absence of ATc or the presence of ATc for 1-3 days, then separated protein extracts by SDS-PAGE. As demonstrated previously, ATc treatment led to depletion of *Tg*ApiCox25 but not of a *Tg*Tom40 loading control (Figure 7E). Interestingly, knockdown of *Tg*ApiCox25 also led to depletion of *Tg*Cox2a-FLAG, although not to the same extent as *Tg*ApiCox25 (Figure 7E). We solubilised proteins from the *Tg*ApiCox25-HA/*Tg*Cox2a-FLAG strain in 1% (v/v) Triton X-100 and separated proteins by blue native PAGE. Knockdown of *Tg*ApiCox25 led to depletion of the ~600 kDa COX complex (Figure 7F). Interestingly, *Tg*ApiCox25 knockdown resulted in the appearance of a ~400 kDa complex that contains *Tg*Cox2a (Figure 7D). Together, these

observations are consistent with *Tg*ApiCox25 having an important role COX complex integrity, stability and/or assembly.

DISCUSSION

In this study, we utilised two spatially-restricted biotin tagging approaches to elucidate the proteome of the mitochondrial matrix of *T. gondii*. These complementary approaches identified 421 putative mitochondrial proteins. This number is slightly lower than the 495 proteins identified in the mtAPEX-derived proteome of mammalian cells (Rhee et al., 2013), and is less than the 750 proteins identified in a yeast study using highly purified mitochondria (Sickmann et al., 2003). Our proteome identified most of the proteins 'expected' to localize to the *T. gondii* mitochondrion (Figure 2D; Supplementary File 3), suggesting a high level of coverage. The lowered numbers of proteins in the *T. gondii* mitochondrial proteome compared to the yeast mitochondrial proteome may represent reduced functions in the parasite organelle compared to that in a metabolically flexible organism such as yeast, although our subsequent analyses (discussed below) are consistent with the presence of a high degree divergent biology in apicomplexan mitochondria.

We experimentally localized 27 previously uncharacterised proteins from the *T. gondii* mitochondrial proteome, finding that 22 of these localised to the mitochondrion (Figure 3). From this, we estimate that ~80% of the 'uncharacterized' proteins from the proteome localize to the mitochondrion. Our findings suggest a low false positive rate in the proteins identified from the APEX proteome alone (~5%), but a higher false positive rate in the mtBirA* proteome (~20%). Based on these analyses, we consider the 213 proteins from the mtAPEX and shared

513 mtAPEX/mtBirA* proteomes to be 'likely' mitochondrial proteins, and the 208 proteins found in
514 the mtBirA* proteome alone to be 'possible' mitochondrial proteins.
515
516 To our knowledge, our study is the first time the APEX and BirA* restricted biotinylation
517 approaches have been directly compared in organellar proteomic approaches. Bioinformatic and
518 localization analyses indicate a high level of overlap between the two approaches, but also
519 indicate the presence of unique proteins in both data sets. This suggests that the two approaches
520 provide complementary information that expands the organellar proteome, while at the same
521 time providing confidence in the shared set of proteins that were identified. The mtBirA*-
522 derived proteome identified greater numbers of proteins, while also featuring greater numbers of
523 false positives. Several recent studies have used BirA* to identify novel proteins in
524 apicomplexan organelles (Boucher et al., 2018; Chen et al., 2015; Kehrer et al., 2016; Nadipuram
525 et al., 2016). Our study is the first time APEX has been used for proteomic applications in
526 apicomplexan parasites, and we suggest that this approach will prove useful in elucidating the
527 proteomes of other apicomplexan organelles (e.g. the apicoplast) or organellar sub-compartments
528 (e.g. the mitochondrial intermembrane space), either by itself or in combination with BirA*
529 approaches. Our study suggests that APEX and BirA* are powerful tools in determining
530 organellar proteomes in apicomplexans.
531
532 Our phylogenetic comparisons suggest that a large number of proteins in the *T. gondii*
533 mitochondrion have homologs in *P. falciparum* (Figure 4A; Supplementary File 1). This is
534 consistent with the presence of similar mitochondrial processes and biochemical pathways in
535 these organisms (Seeber et al., 2008). The lower value in *C. parvum* is consistent with the

536 reduced function of the mitosome of this organism (Mogi and Kita, 2010). The shared
537 mitochondrial/mitosomal proteome of *T. gondii* and *C. parvum* likely consists of proteins
538 involved in pathways shared between these organisms, such as Fe-S cluster synthesis. Notably,
539 we identified homologs to 83% of *T. gondii* mitochondrial proteins in the chromerid *V.*
540 *brassicaformis* (Figure 4A; Supplementary File 1). This mirrors recent findings that several
541 'derived' features of apicomplexan mitochondria, including the repurposing of the BCKDH, the
542 loss of Complex I and the acquisition of novel TCA cycle enzymes, were already present in the
543 free-living, autotrophic common ancestor of myzozoans (dinoflagellates, chromerids and
544 apicomplexans; (Danne et al., 2013; Jacot et al., 2015)). Notably, most of the ApiCox proteins
545 we identified in the *T. gondii* COX complex had homologs in chromerids (Table 1), indicating
546 that even conserved mitochondrial processes in this group of organisms have a considerable
547 degree of novelty. Together, these data indicate that much of the mitochondrial biology in *T.*
548 *gondii* was present in the free-living ancestor that they share with chromerids.
549
550 Many (~40-50%) mitochondrial proteins in *T. gondii* lack apparent orthologs in animals and
551 other eukaryotes (Figure 4B-C). Surprisingly, proteins found only in coccidians, or restricted to
552 apicomplexans and chromerids, were just as likely to be important for parasite growth as proteins
553 conserved across eukaryotic evolution (Figure 4D). This suggests that many derived or unique
554 features of the *T. gondii* mitochondrion (and apicomplexan mitochondria more generally) are
555 critical for parasite survival. This is in contrast to the general proteome of *T. gondii*, where
556 proteins with a restricted phylogenetic distribution are typically less important for parasite
557 survival (Sidik et al., 2016).
558

559 To understand the functions of apicomplexan-specific mitochondrial proteins that are important
560 for parasite growth, we have commenced a project to characterize these proteins. In this study,
561 we describe the characterisation of *Tg*ApiCox25, demonstrating that this is a component of the *T.*
562 *gondii* COX complex. *Tg*ApiCox25 is important for parasite growth and mitochondrial oxygen
563 consumption (Figure 5). Knockdown of *Tg*ApiCox25 also leads to defects in the integrity of the
564 COX complex. In particular, *Tg*ApiCox25 knockdown leads to a depletion of *Tg*Cox2a
565 abundance, and also results in the appearance of a smaller, ~400 kDa *Tg*Cox2a-containing
566 complex (Figure 7E-F). These data imply an important role for *Tg*ApiCox25 in the assembly
567 and/or stability of the COX complex. It remains unclear whether loss of *Tg*ApiCox25 leads to
568 loss of a ~200 kDa module from the complex, or whether *Tg*ApiCox25 knockdown leads to
569 defects in COX assembly, with the ~400 kDa complex representing an assembly intermediate.
570 Regardless, loss of *Tg*ApiCox25 results in defects in the abundance and integrity of the parasite
571 COX complex, which likely explains the defects in mOCR observed upon *Tg*ApiCox25
572 knockdown. Future studies will examine the functional role of *Tg*ApiCox25 in the COX complex
573 of the parasite.
574
575 Our analysis of the parasite COX complex revealed that it is approximately 600 kDa in mass
576 (Figures 6A), which is larger than the equivalent complex in yeast (200 kDa), mammals (200
577 kDa) and plants (220/300 kDa) (Eubel et al., 2003; Lenaz and Genova, 2010; Marechal et al.,
578 2012; Schagger and Pfeiffer, 2000; Tsukihara et al., 1996). It is conceivable that the *T. gondii*
579 COX complex exists in a multimeric form (e.g. a homodimer or homotrimer), and/or that it
580 contains subunits not present in the complex of these other organisms that inflate its mass.
581 Another possibility is that *T. gondii* COX exists in a 'super-complex' with other respiratory

582 complexes, as has been observed in other systems (Eubel et al., 2003; Schagger and Pfeiffer,
583 2000). Although we cannot rule out that respiratory chain supercomplexes exist in *T. gondii*, the
584 600 kDa complex is probably not a supercomplex, since we do not observe enrichment of
585 canonical components of other respiratory chain proteins in our proteomic analysis of the
586 complex, and the molecular masses of other respiratory chain complexes in *T. gondii* do not
587 correspond in size to COX (GvD, unpublished observations).
588
589 We identified 12 proteins in the *T. gondii* COX complex. In addition to these, it is likely that the
590 complex contains *Tg*CoxI and *Tg*CoxIII, proteins encoded on the mitochondrial genome of the
591 parasite. Although excluded from our statistical analysis due to its absence from the control
592 dataset, a CoxIII homolog was enriched in the *Tg*ApiCox25 immunoprecipitation
593 (Supplementary File 5). 14 COX proteins in *T. gondii* is comparable in number to those found in
594 the mammalian (13 proteins) and plant (10 or 12 proteins) complexes (Eubel et al., 2003;
595 Tsukihara et al., 1996). Surprisingly, only a few *T. gondii* COX proteins have obvious homologs
596 in eukaryotes outside the myzozoan lineage. Of note, 8 of the 9 ApiCox proteins we identified
597 have homologs in chromerids (Table 1), while none of these have clear homologs in ciliates
598 (http://orthomcl.org), the eukaryotic lineage that is the sister taxon to myzozoans. This
599 suggests either a high degree of novelty in the proteins that comprise the *T. gondii*/myzozoan
600 COX complex, or that the sequences of ApiCox proteins have diverged to the extent that they are
601 no longer easily recognisable by sequence comparisons. Notably, similarity searches that
602 incorporate secondary structure information suggest that ApiCox25 and ApiCox23 may have
603 homology to Cox6a and Cox4, respectively, from animals. A priority in the field is to establish
604 the structure of the COX complex in myzozoans, which will reveal whether ApiCox proteins

have structural equivalents in other eukaryotes. Regardless of their degree of novelty, our observations are consistent with other observations that suggest a considerable divergence in the mitochondrial biology of organisms in the myzozoan lineage compared to other eukaryotes (Danne et al., 2013; Jacot et al., 2015).

Our study highlights the divergence of mitochondrial proteomes across the eukaryotic domain of life. Future studies will be aimed at elucidating the function of other *T. gondii*- and myzozoan-specific mitochondrial proteins, since these proteins will provide insights into unique functions of the organelle. Given their importance to parasite growth, and their absence (or divergence) from the host organisms that they infect, these *T. gondii* and apicomplexan-specific proteins are prime drug targets.

MATERIALS AND METHODS

Parasite culture. *T. gondii* parasites were passaged in human foreskin fibroblasts (HFF), and cultured in Dulbecco's Modified Eagle's Medium, supplemented with 1% (v/v) fetal bovine serum and antibiotics. Where appropriate, ATc was added to a final concentration of 0.5 µg/ml. Plaque assays were performed as described previously (van Dooren et al., 2008), with plaque sizes measured using ImageJ.

Plasmid construction and parasite transfection. To generate a *T. gondii* strain expressing mitochondrial matrix-targeted APEX, we amplified the coding sequence of monomeric APEX using the primers 5'-GACTCCTAGGGGAAAGTCTTACCCAACT and 5'-

GACTCATATGGGCATCAGCAAACCCAAG, and the vector pcDNA3-mito-APEX as template (a gift from Alice Ting; Addgene plasmid # 42607; (Martell et al., 2012)). The resultant PCR product was digested with *Avr*II and *Nde*I and ligated into equivalent sites of the vector $Hsp60_L$-mDHFR in $pBTM_3$ (van Dooren et al., 2016). This fuses the mitochondrial targeting sequence of *Tg*Hsp60 to 3x c-myc-tagged APEX. The resultant vector was transfected into RHΔ*hxgprt* strain *T. gondii* parasites, and selected on phleomycin as described (Messina et al., 1995). To generate a *T. gondii* strain expressing a mitochondrial matrix-targeted BirA*, we amplified the coding sequence of BirA* using the primers 5'-GATCAGATCTAAAATGCCTAGGGGTTCTGGCGGTGACAAGGACAACACCG and 5'-GATCTCTAGACTTCTCTGCGCTTCTCAGGGAGA and the vector pBirA*-3XHA-LIC-DHFR as template ((Chen et al., 2015); a gift from Peter Bradley, University of California Los Angeles). The resultant product was digested with *Bgl*II and *Xba*I and ligated into the *Bgl*II and *Avr*II sites of pgCM3 (GvD, unpublished). The BirA*-3x c-myc cassette of the resultant vector was digested with *Avr*II and *Not*I and ligated into the equivalent sites of the $Hsp60_L$-mDHFR in $pBTM_3$ vector. This fuses the mitochondrial targeting sequence of *Tg*Hsp60 to 3x c-myc-tagged BirA*. The resultant vector was transfected into RHΔ*hxgprt* strain *T. gondii* parasites, and selected on phleomycin.

For localising candidate mitochondrial proteins from the proteome (including *Tg*ApiCox25 and *Tg*ApiCox30), we amplified the 3' region of 27 target genes using the primers listed in Supplementary File 4. We digested resultant PCR products with enzymes suitable for subsequent ligation into the *Spe*I, *Bgl*II and/or *Avr*II sites of the vector pgCH (Rajendran et al., 2017), as outlined in Supplementary File 4. The resulting vector was linearized with an enzyme that cut

651 once in the flanking sequence, transfected into TATi/Δ*ku80* strain parasites (Sheiner et al.,
652 2011), and selected on chloramphenicol as described (Striepen and Soldati, 2007). The resultant
653 parasite strains have a 1xHA tag fused to the 3' end of the open reading frame of the target gene,
654 enabling subsequent localisation of the target protein by immunofluorescence assays.
655
656 To introduce an ATc-regulated promoter into the *Tg*ApiCox25 locus, we generated a vector
657 expressing a sgRNA targeting the region around the start codon of *Tg*ApiCox25. To do this, we
658 modified the vector pSAG1::Cas9-U6::sgUPRT (Addgene plasmid # 54467; (Shen et al., 2014))
659 using Q5 site-directed mutagenesis (New England Biolabs) as described previously (Shen et al.,
660 2014). For site-directed mutagenesis, we used the primers 5'-
661 TCACGTGTAAACAGGGGAGTGTTTTAGAGCTAGAAATAGCAAG (sgRNA region
662 specific to the *Tg*ApiCox25 is underlined) and the universal reverse primer 5'-
663 AACTTGACATCCCCATTTAC. We also PCR amplified the ATc-regulated promoter plus a
664 'spacer' region consisting of part of the *T. gondii* DHFR open reading frame and 3' UTR using
665 the pPR2-HA3 vector (Katris et al., 2014) as template and the primers 5'-
666 GCCTGGCATAAAATTCGGGGACTGATTTCTCCACGTCACGTGTAAACAGGGGTTGCA
667 GGCTCCTTCTTCGG and 5'-
668 ACGATCGGCGCTCCGGCGAAGCGGAGTAGTAAAGATGTCCGCAACATCTTGGTTGA
669 AGACAGACGAAAGCAGTTG, which each contain 50 bp of sequence specific for the
670 *Tg*ApiCox25 locus. The sgRNA expressing vector, which also expressed GFP-tagged Cas9, was
671 co-transfected into TATi/Δ*ku80* strain parasites along with the ATc-regulatable promoter as
672 described (Striepen and Soldati, 2007). GFP-positive parasites were selected and cloned 3 days
673 following transfection. Clones were screened for successful integration of the ATc-regulatable

674 promoter using the primers *Tg*ApiCox25 fwd (5'-CGTAGGAAAACTGTTCCCAGAGC) and
675 *Tg*ApiCox25 rvs (5'-GCACTTCTTCTGAAAGTTGATACG), or t7s4 fwd (5'-
676 ACGCAGTTCTCGGAAGACG) and *Tg*ApiCox25 rvs.
677
678 To generate a vector that constitutively expressed *Tg*ApiCox25 for complementing the
679 r*Tg*ApiCox25 mutant, we PCR amplified the *Tg*ApiCox25 open reading frame with the primers
680 5'-CATGGGATCCAAAATGTTGCGGACATCTTTACTACTCC and 5'-
681 CATGCCTAGGGTGAAAGTGAGGTGGCTCCAGTT. We digested the resulting PCR product
682 with *Bam*HI and *Avr*II and ligated this into the *Bgl*II and *Avr*II sites of the vector pUgCTH$_3$
683 (Rajendran et al., 2017). The resulting vector was linearized with *Mfe*I, transfected into
684 r*Tg*ApiCox25 parasites, and selected on chloramphenicol as described (Striepen and Soldati,
685 2007).
686
687 To FLAG tag the native locus of *Tg*Cox2a, we generated a vector expressing a sgRNA targeting
688 the region around the stop codon of *Tg*Cox2a. To do this, we modified the pSAG1::Cas9-
689 U6::sgUPRT vector using Q5 mutagenesis with the primer 5'-
690 CGAGTCGCCTGTTGACGACGGTTTTAGAGCTAGAAATAGCAAG (gene-specific region
691 of the sgRNA underlined) and the universal reverse primer (as described above). We also
692 amplified a FLAG tag containing 50 bp of flanking sequence either side of the *Tg*Cox2a stop
693 codon, using the primers 5'-
694 GACAGTGGTACTGGATCTACGAAGTCGAGTCGCCTGTTGACGACGAAGAGGGTGGA
695 GGTAGCGGTGGTGGAAG and 5'-
696 CTGCCCATTCAACGCTCGGACAGCCGTCCTTTAGGAAACGCATAGGAAGCGCTTCTG

TGGGCGGTTATCAGG, with FLAG template synthesized as a gBlock (IDT). The FLAG tag gBlock sequence was as follows: 5'-GTGGAGGTAGCGGTGGTGGAAGTGACTACAAAGACCATGACGGTGATTATAAAGATCATGACATCGATTACAAGGATGACGATGACAAGTAGTCCTGATAACCGCCCACAGAAGC. We co-transfected the plasmid and PCR product into *Tg*ApiCox25-HA or r*Tg*ApiCox25-HA strain parasites, selected GFP positive parasites by flow cytometry 3 days post-transfection, then screened for successful integrants using the primers 5'-CTCTTGTACATGCTCGACGAAG and 5'-AACGACTGTGATTCCAAAACCT.

To FLAG tag the native locus of *Tg*ApiCox25, we generated a vector expressing a sgRNA targeting the region around the stop codon of TgApiCox25, modifying the pSAG1::Cas9-U6::sgUPRT vector using Q5 mutagenesis with the primer 5'-TGTCTTCAGTGAAAGTGAGGGTTTTAGAGCTAGAAATAGCAAG (gene-specific region of the sgRNA underlined) and the universal reverse primer (described above). We also amplified a FLAG tag containing 50 bp of flanking sequence either side of the *Tg*ApiCox25 stop codon, using the primers 5'-GAAATCCCCTCTCTGTTCCTAGAGGCAAACTGGAGCCACCTCACTTTCACGGTGGAGGTAGCGGTGGTGGAAG and 5'-ACACAAGGATCGCATACCATAGCACGCAACACAAACAGTCATTGTTTGAGGCTTCTGTGGGCGGTTATCAGG, and the FLAG gBlock (described above) as template. We co-transfected the plasmid and PCR product into *Tg*ApiCox30-HA strain parasites, selected GFP positive parasites by flow cytometry 3 days post-transfection, then screened for successful

719 integrants using the primers 5'-GATGAGTCGTCTGTGGTTCATTG and *Tg*ApiCox25 rvs
720 (described above).
721
722 **Synthesis of biotin-phenol.** Biotin phenol was synthesised as described previously (Rhee et al.,
723 2013). 50 mg/ml biotin (Sigma) was slowly mixed with 1.1 equivalents of 2-(7-aza-1H-
724 benzotriazole-1-yl)-1,1,3,3-tetramethyluronium (Sigma) and 3.0 equivalents of N,N-
725 diisopropylethylamine (Sigma). The mixture was stirred for 10 min at room temperature, then
726 1.0 equivalent of tyramine (Sigma) was added slowly. The resulting solution was stirred
727 overnight at room temperature. The synthesised biotin-phenol was purified from the unreacted
728 material with a Reveleris flash chromatography system (Grace, MD, USA) and a C18-WP 4g
729 column, using an acetonitrile/water gradient. Eluting compounds were monitored with a UV
730 detector (220 nm, 278 nm, and 350 nm) and an evaporative light scattering detector (ELSD)
731 coupled to the flash chromatography system. The eluted biotin-phenol in acetonitrile/water
732 mixture was freeze-dried and reconstituted in dimethyl sulfoxide at a final concentration of 200
733 mM. The purity of biotin-phenol was confirmed by ultra-high performance liquid
734 chromatography (UHPLC, Dionex).
735
736 **Biotinylation approaches.** For biotin-phenol labelling, freshly egressed wild type or mtAPEX-
737 expressing parasites were resuspended in parasite growth medium. Biotin-phenol was added to
738 the parasites at final concentration of 1 mM, and parasites were incubated at 37°C for 1 hr.
739 Biotinylation was initiated by the addition of 1 mM H_2O_2 for 45 sec, and halted by centrifuging
740 cells at 12,000g for 30 sec. The medium was removed, and parasite cells were washed three
741 times in quenching solution (10mM sodium azide, 10mM sodium ascorbate, and 5mM Trolox in

742 phosphate-buffered saline (PBS)), and once in PBS. Cell pellets were stored at -80°C until
743 further processing.
744
745 For biotin-labelling, host cells were infected with wild type or mtBirA*-expressing parasites.
746 Biotin was added to infected host cells ~48 hours after infection, to a final concentration of 1
747 mM. Infected host cells were cultured for a further 24 hours, during which time they naturally
748 egressed from host cells. Parasites were harvested by centrifugation at 1500 g and washed 3
749 times in PBS. Cell pellets were stored at -80°C until further processing.
750
751 Biotin treated parasite pellets were lysed in radioimmunoprecipitation assay (RIPA) buffer
752 (50mM Tris, 150 mM NaCl, 0.1% (w/v) SDS, 0.5% (w/v) sodium deoxycholate, 1% (v/v) Triton
753 X-100, Complete protease cocktail (Roche)) for 30 min on ice. Biotin-phenol treated parasite
754 pellets were lysed in RIPA buffer containing quenching agents (10 mM sodium azide, 10mM
755 sodium ascorbate, and 5 mM Trolox). 3 independent lysate pools of WT parasites treated with
756 biotin-phenol and H_2O_2, mtAPEX-expressing parasites treated with biotin-phenol and H_2O_2, WT
757 parasites treated with biotin, and mtBirA*-expressing parasites treated with biotin were
758 generated, and protein concentration was quantified using Bradford reagent (Sigma).
759
760 For enrichment of biotinylated proteins with streptavidin beads, 8 mg of protein from each pool
761 was diluted with RIPA buffer to reach 1.8 ml total volume. 223 µl of streptavidin-conjugated
762 magnetic beads (Thermo Scientific) per pool was dispensed in 2 ml microcentrifuge tubes. A
763 magnabind magnet (Thermo Scientific) was used to separate beads from the buffer solution.
764 Beads were washed three times in RIPA buffer, and incubated with the corresponding lysate

765 pools for 1 hr at room temperature with gentle rotation. The beads were then washed three times
766 in RIPA buffer, once with 2M urea in 10 mM Tris-HCl pH 8.0, and a further three times in RIPA
767 buffer. The resin-bound proteins were treated with reducing solution (10mM DTT in 100mM
768 ammonium bicarbonate) for 30 min at 56°C. The reducing solution was removed, and replaced
769 with alkylation solution (55 mM iodoacetamide in 100 mM ammonium bicarbonate) and
770 incubated at room temperature in the dark for 45 min. The alkylation solution was then removed,
771 and the beads were washed in 50mM ammonium bicarbonate for 15 min with gentle agitation.
772 The ammonium bicarbonate solution was removed, and samples treated with 20 ng/µl
773 sequencing grade trypsin (Promega) overnight (18 hrs) at 37°C. The next day, the supernatant
774 was collected and beads were further treated with 10 % (v/v) formic acid, and incubated for 15
775 min at 37°C.
776
777 The volume of peptide filtrates was reduced to ~12 µl in a centrifugal evaporator. Zip tips
778 containing 0.6 µl C18 resin (Millipore) were washed with 10 µl methanol, and 10 µl 0.1% (v/v)
779 formic acid. The digested peptides were loaded onto the tips by pipetting the peptide solutions 10
780 times. The tips were then washed with 10 µl 0.1% (v/v) formic acid twice, and the peptides were
781 eluted into Chromacol 03-FISV vials with conical 300 µl inserts using 50% acetonitrile/0.1%
782 formic acid (v/v), and dried in a vacuum concentrator.
783
784 MS analysis was performed on a Q-Exactive Classic mass spectrometer as previously described
785 (Delconte et al., 2016). Raw files consisting of high-resolution MS/MS spectra were processed
786 with MaxQuant (version 1.5.2.8) for feature detection and protein identification using the
787 Andromeda search engine (Cox et al., 2011). Extracted peak lists were searched against the

UniProtKB/Swiss-Prot *Homo sapiens* and *Toxoplasma gondii* ME49 (ToxoDB-12.0) databases and a separate reverse decoy database to empirically assess the false discovery rate (FDR) using strict trypsin specificity allowing up to 3 missed cleavages. The minimum required peptide length was set to 7 amino acids. *Modifications:* Carbamidomethylation of Cys was set as a fixed modification, while N-acetylation of proteins and oxidation of Met were set as variable modifications. The mass tolerance for precursor ions and fragment ions were 20 ppm and 0.5 Da, respectively. The "match between runs" option in MaxQuant was used to transfer identifications made between runs on the basis of matching precursors with high mass accuracy (Cox and Mann, 2008). PSM and protein identifications were filtered using a target-decoy approach at a false discovery rate (FDR) of 1%.

Quantitative proteomics pipeline. Statistically-relevant protein expression changes were identified using a custom pipeline as previously described (Delconte et al., 2016). Probability values were corrected for multiple testing using Benjamini–Hochberg method. Cut-off lines with the function $y= -\log_{10}(0.05)+c/(x-x_0)$ (Keilhauer et al., 2015) were introduced to identify significantly enriched proteins. c was set to 0.2 while x_0 was set to 1 representing proteins that are differentially expressed within 1 or 2 standard deviations.

Bioinformatic analyses of data. Homologs of *T. gondii* mitochondrial proteome proteins were identified in the apicomplexan parasites *P. falciparum* (strain 3D7), *C. parvum* and *B. bovis*, and the chromerid *V. brassicaformis*, through reciprocal Basic Local Alignment Search Tool (BLAST) searches. *T. gondii* mitochondrial proteome proteins were used as query sequences in initial searches using target protein databases from relevant EupathDB websites

(http://PlasmoDB.org– *P. falciparum*; http://PiroplasmaDB.org – *Babesia bovis*; http://CryptoDB.org – *Cryptosporidium parvum* and *Vitrella brassicaformis*; (Aurrecoechea et al., 2013)). Hits from the initial BLAST search were queried in reciprocal BLAST searches against the *T. gondii* genome database (http://toxodb.org), regardless of the score or E-value obtained. Hits that returned the corresponding *T. gondii* protein that was originally searched against were considered as a homolog. Expect (E) values obtained from the initial BLAST search and the reciprocal BLAST search were recorded (Supplementary File 1). Homologs of proteins identified in the purified ApiCox25 complex were identified using the profile hidden Markov model search tool HMMER (https://www.ebi.ac.uk/Tools/hmmer/).

Ortholog grouping for each protein was obtained from ToxoDB. Each ortholog group was assessed for the presence of ortholog proteins in other eukaryotic organisms based on the phyletic information available on http://OrthoMCL.org (Chen et al., 2006). Information of ortholog grouping for the entire genome of the chromerid *V. brassicaformis* were sourced from CryptoDB, and were subsequently compared to the ortholog groups identified for the *T. gondii* mitochondrial proteome. HHPRED predictions were performed using the MPI Bioinformatics Toolkit website (https://toolkit.tuebingen.mpg.de/#/tools/hhpred; (Zimmermann et al., 2017)).

The presence of predicted mitochondrial targeting peptides was assessed using MitoProt (Claros and Vincens, 1996), with the probability of export into the mitochondria recorded (Supplementary File 1). Metabolic pathway enrichment was assessed using the Metabolic Pathway search tool on ToxoDB, using a p value cut-off of <0.05.

834 **Immunofluorescence assays and microscopy.** IFAs were performed as described previously
835 (van Dooren et al., 2008). Primary antibodies used were mouse anti-c-myc (1:200 dilution; Santa
836 Cruz clone 9E10), rat anti-HA (1:200 dilution; Sigma clone 3F10), and rabbit anti-Tom40
837 (1:2000 dilution; (van Dooren et al., 2016)). Secondary antibodies used were goat anti-mouse
838 Alexa Fluor 488 (1:500 dilution; Life Technologies), goat anti-rat Alexa Fluor 488 (1:100 to
839 1:500 dilution; Life Technologies), goat anti-rat CF 488A (1:100 to 1:500 dilution; Sigma), and
840 goat anti-rabbit Alexa Fluor 546 (1:500 dilution; Life Technologies). Biotinylation was
841 performed as outlined for the proteomics, except that mtAPEX samples were incubated in H_2O_2
842 for 1 min. For visualising biotinylated proteins, we used Oregon Green-conjugated avidin
843 (1:1,000 dilution; Life Technologies). Images were acquired on a DeltaVision Elite
844 deconvolution microscope (GE Healthcare) fitted with a 100X UPlanSApo oil immersion
845 objective lens (NA 1.40). Images were deconvolved and adjusted for contrast and brightness
846 using SoftWoRx Suite 2.0 software, and subsequently processed using Adobe Illustrator.
847
848 **Immunoprecipitations.** Immunoprecipitations were performed as described previously (van
849 Dooren et al., 2016), except that parasite samples were solubilized in 1% (v/v) Triton X-100.
850 HA-tagged proteins were purified using anti-HA affinity matrix (Sigma; rat anti-HA clone 3F10
851 antibodies) and FLAG-tagged proteins were purified using anti-FLAG M2 affinity gel (Sigma;
852 mouse anti-FLAG clone M2 antibodies). For mass spectrometry sample preparation, anti-HA
853 beads bound with HA-tagged protein complexes were frozen at -80°C for 1 hr, then eluted at
854 37°C in 0.2 M glycine containing 1% (v/v) Triton X-100 (pH 2.3). Samples were neutralized in
855 ammonium bicarbonate, then extracted in chloroform:methanol as described (Pankow et al.,
856 2016). After extraction, the pellets were dried and stored at -80°C before mass spectrometry

857 analysis at the Mass Spectrometry Facility, La Trobe University Institute for Molecular Science.
858 Peptides were searched against the UniProt TOXGV (*T. gondii*) database using strict trypsin
859 specificity allowing up to 2 missed cleavages. *Modifications:* Carbamidomethylation of Cys was
860 set as a fixed modification, and N-acetylation of proteins and oxidation of Met were set as
861 variable modifications. The mass tolerance for fragment ions was 0.5 Da. Statistical validation of
862 peptide spectra matches was performed using PeptideProphet.
863
864 **SDS-PAGE, Blue Native-PAGE and immuno/affinity-blotting.** SDS-PAGE and protein
865 blotting were performed as described previously (van Dooren et al., 2008), except that
866 membranes used for neutravidin blotting were blocked with 3 % (w/v) bovine serum albumin
867 (BSA). Blue native PAGE was performed using the NativePAGE system (Thermo Scientific) as
868 described previously (van Dooren et al., 2016). Blots were probed with antibodies against mouse
869 anti-c-myc (1:500 dilution; Santa Cruz clone 9E10), rabbit anti-Hsp60 (1:1000 dilution; (Tonkin
870 et al., 2004)), rabbit anti-*T. gondii* cyt *c* (1:500 dilution; E.T. and G.v.D., unpublished), rat anti-
871 HA (1:500 to 1:1000 dilution; Sigma clone 3F10), mouse anti-FLAG (1:500 to 1:2000 dilution;
872 Sigma clone M2), and rabbit anti-AtpB (1:500; Agrisera, catalog number AS05 085).
873 Horseradish peroxidase (HRP)-conjugated anti-mouse, anti-rat and anti-rabbit antibodies (Santa
874 Cruz) were used at 1:5,000 dilution. For probing for mouse antibodies on immunoprecipitation
875 western blots, HRP-conjugated anti-mouse TrueBlot ULTRA antibodies (eBioscience) were used
876 at 1:5,000 dilution. Neutravidin-HRP (Life Technologies) was used to detect biotinylated
877 proteins on membranes at 1:10,000 dilution.
878

Seahorse XFe96 Extracellular flux analysis. Wild type (TATi/Δ*ku80*) and r*Tg*ApiCox25 parasites were grown in the absence of ATc, in the presence of ATc for 1-3 days, or with 100 µM cycloheximide for 1 day. Parasites were filtered through a 3 µm polycarbonate filter and washed twice in Seahorse XF base medium (Agilent Technologies), supplemented with 1 mM L-glutamine and 5 mM D-glucose (supplemented base medium), before resuspension to 1.5 x 10^7 cells/ml in the supplemented base medium. 96-well Seahorse culture plates were coated with 3.5 µg/cm^2 of CellTak cell adhesive (Corning) according to the manufacturer's instructions. Briefly, 1mg/ml CellTak was diluted 1:50 in 0.1 M sodium bicarbonate. 15 µl of CellTak solution was added to each well of a Seahorse cell culture plate and incubated at RT for 20 mins. The solution was removed and the plate washed twice in sterile water, before drying. 100 µl of the parasite suspensions (1.5 x 10^6 parasites) were seeded into wells of the coated plate, and the plate was centrifuged at 50 g for 3 min. An additional 75 µL of supplemented base medium was added to each well following centrifugation. Parasites were kept at 37°C in a non-CO_2 incubator until the start of experiment. Parasite oxygen consumption rates (OCR) and extracellular acidification rates (ECAR) were measured using an Agilent Seahorse XFe96 Analyzer at 3 minute intervals. To determine the maximal OCR, parasites were treated with 20 µM oligomycin A, B and C mix (Sigma) to inhibit ATP synthase, then subsequently treated with 1 µM carbonyl cyanide-4-(trifluoromethoxy)phenylhydrazone (FCCP; Sigma). To determine the non-mitochondrial OCR, parasites were treated with 10 µM antimycin A (Sigma) and 1 µM atovaquone (the minimal concentration that preliminary experiments indicated is sufficient to maximally inhibit mitochondrial OCR). The mitochondrial OCR (mOCR) was calculated by subtracting the non-mitochondrial OCR from the basal and maximal OCR values. A minimum of 4 wells were used

for background correction in each assay plate, and 4-5 technical replicates were used for each condition. Wells that yielded negative OCR values were excluded from the final analysis.

Miscellaneous data analysis. XFe96 data were compiled using the Wave Desktop program. Analysis of parasite OCR and ECAR were performed using the R software environment (Source Code File 1). Linear mixed-effects models were fitted to the data, with error between plates and wells (i.e. between and within experiments) defined as the random effect, and the OCR and ECAR measurements in the different parasite strains (WT and r*Tg*ApiCox25) and the time since ATc-addition defined as the fixed effect. Data from the *Tg*ApiCox25-HA and *Tg*Tom40-HA co-immunopreciptation proteomics were analysed in the R software environment using the EdgeR package (Source Code File 2; (Robinson and Smyth, 2008)). Only proteins identified in both experimental conditions and each biological replicate were included in the final analysis. Graphing of the XFe96 and *Tg*ApiCox25 proteomic data were performed in GraphPad Prism v. 7.0.

Data Availability. The mitochondrial proteome data are available on individual gene pages on the ToxoDB website (http://toxodb.org), and a "Mitochondrial Matrix Quantitative Proteome" search tool is available in the proteomics section of ToxoDB (https://bit.ly/2FySSmU). To use the search tool, first select the **experiment** that you want to query. "Control APEX vs mito APEX" queries the APEX data, and "Control BirA vs mito BirA" queries the BirA* data. Next select the **direction** of the query. To examine genes that are enriched in the mitochondrial matrix proteomes, select "down-regulated" (i.e. proteins that are less abundant in control samples than in the mito APEX/BirA* samples). Next select the desired **P value**. For our analyses, we utilised

924 a P value of ≤0.001. Finally, select the desired **fold difference**. For our analyses, we utilised a
925 $\log_2$ fold change value of ≥ 2.5, which corresponds to a fold change of ≥ 5.657.
926
927 **ACKNOWLEDGEMENTS**
928 We thank Peter Bradley (UCLA) and Alice Ting (Stanford) for sharing reagents, Pierre Faou (La
929 Trobe) for proteomic analysis of the *Tg*ApiCox25 complex, Michael Devoy and Harpreet Vohra
930 (ANU) for assistance with flow cytometry, Michael Devoy (ANU) for assistance in establishing
931 the Seahorse XFe96 assays, Teresa Neeman from the ANU Statistical Consulting Unit for
932 assistance with data analysis, and Sebastian Lourido (Whitehead Institute) for comments on the
933 manuscript. We are grateful to EuPathDB for providing numerous datasets and search tools, and
934 in particular to Susanne Warrenfeltz for co-ordinating the integration of the mitochondrial matrix
935 proteomic data into ToxoDB. This work was supported by a Discovery Grant and QEII
936 fellowship from the Australian Research Council (ARC DP110103144) to G.v.D.
937

REFERENCES

Aurrecoechea, C., Barreto, A., Brestelli, J., Brunk, B.P., Cade, S., Doherty, R., Fischer, S., Gajria, B., Gao, X., Gingle, A., *et al.* (2013). EuPathDB: the eukaryotic pathogen database. Nucleic Acids Res *41*, D684-691. doi:10.1093/nar/gks1113

Balabaskaran Nina, P., Morrisey, J.M., Ganesan, S.M., Ke, H., Pershing, A.M., Mather, M.W., and Vaidya, A.B. (2011). ATP synthase complex of *Plasmodium falciparum*: dimeric assembly in mitochondrial membranes and resistance to genetic disruption. J Biol Chem *286*, 41312-41322. doi:10.1074/jbc.M111.290973

Boucher, M.J., Ghosh, S., Zhang, L., Lal, A., Jang, S.W., Ju, A., Zhang, S., Wang, X., Ralph, S.A., Zou, J., *et al.* (2018). The proteome of the malaria plastid organelle, a key anti-parasitic target. bioRxiv. doi:10.1101/265967

Brydges, S.D., and Carruthers, V.B. (2003). Mutation of an unusual mitochondrial targeting sequence of SODB2 produces multiple targeting fates in *Toxoplasma gondii*. J Cell Sci *116*, 4675-4685.

Cavalier-Smith, T., and Chao, E.E. (2004). Protalveolate phylogeny and systematics and the origins of Sporozoa and dinoflagellates (phylum Myzozoa nom. nov.). Eur J Protistol *40*, 185-212.

Chen, A.L., Kim, E.W., Toh, J.Y., Vashisht, A.A., Rashoff, A.Q., Van, C., Huang, A.S., Moon, A.S., Bell, H.N., Bentolila, L.A., *et al.* (2015). Novel components of the *Toxoplasma* inner membrane complex revealed by BioID. MBio *6*, e02357-02314. doi:10.1128/mBio.02357-14

Chen, F., Mackey, A.J., Stoeckert, C.J., Jr., and Roos, D.S. (2006). OrthoMCL-DB: querying a comprehensive multi-species collection of ortholog groups. Nucleic Acids Res *34*, D363-368. doi:10.1093/nar/gkj123

Chernikova, D., Motamedi, S., Csuros, M., Koonin, E.V., and Rogozin, I.B. (2011). A late origin of the extant eukaryotic diversity: divergence time estimates using rare genomic changes. Biol Direct *6*, 26. doi:10.1186/1745-6150-6-26

Claros, M.G., and Vincens, P. (1996). Computational method to predict mitochondrially imported proteins and their targeting sequences. Eur J Biochem *241*, 779-786.

Cox, J., and Mann, M. (2008). MaxQuant enables high peptide identification rates, individualized p.p.b.-range mass accuracies and proteome-wide protein quantification. Nat Biotechnol *26*, 1367-1372. doi:10.1038/nbt.1511

Cox, J., Neuhauser, N., Michalski, A., Scheltema, R.A., Olsen, J.V., and Mann, M. (2011). Andromeda: a peptide search engine integrated into the MaxQuant environment. J Proteome Res *10*, 1794-1805. doi:10.1021/pr101065j

Danne, J.C., Gornik, S.G., Macrae, J.I., McConville, M.J., and Waller, R.F. (2013). Alveolate mitochondrial metabolic evolution: dinoflagellates force reassessment of the role of parasitism as a driver of change in apicomplexans. Mol Biol Evol *30*, 123-139. doi:10.1093/molbev/mss205

Delconte, R.B., Kolesnik, T.B., Dagley, L.F., Rautela, J., Shi, W., Putz, E.M., Stannard, K., Zhang, J.G., Teh, C., Firth, M., *et al.* (2016). CIS is a potent checkpoint in NK cell-mediated tumor immunity. Nat Immunol *17*, 816-824. doi:10.1038/ni.3470

Ding, M., Kwok, L.Y., Schluter, D., Clayton, C., and Soldati, D. (2004). The antioxidant systems in *Toxoplasma gondii* and the role of cytosolic catalase in defence against oxidative injury. Mol Microbiol *51*, 47-61. doi:3823 [pii]

983 Doggett, J.S., Nilsen, A., Forquer, I., Wegmann, K.W., Jones-Brando, L., Yolken, R.H., Bordon,
984 C., Charman, S.A., Katneni, K., Schultz, T.*, et al.* (2012). Endochin-like quinolones are
985 highly efficacious against acute and latent experimental toxoplasmosis. Proc Natl
986 Acad Sci U S A *109*, 15936-15941. doi:10.1073/pnas.1208069109
987 Eubel, H., Jansch, L., and Braun, H.P. (2003). New insights into the respiratory chain of plant
988 mitochondria. Supercomplexes and a unique composition of complex II. Plant Physiol
989 *133*, 274-286.
990 Feagin, J.E., Harrell, M.I., Lee, J.C., Coe, K.J., Sands, B.H., Cannone, J.J., Tami, G., Schnare, M.N.,
991 and Gutell, R.R. (2012). The fragmented mitochondrial ribosomal RNAs of
992 *Plasmodium falciparum*. PLoS One *7*, e38320. doi:10.1371/journal.pone.0038320
993 Ferrick, D.A., Neilson, A., and Beeson, C. (2008). Advances in measuring cellular
994 bioenergetics using extracellular flux. Drug Discov Today *13*, 268-274.
995 doi:10.1016/j.drudis.2007.12.008
996 Foth, B.J., Stimmler, L.M., Handman, E., Hodder, A.N., Crabb, B.S., and McFadden, G.I. (2005).
997 The malaria parasite *Plasmodium falciparum* has only one pyruvate dehydrogenase
998 complex, which is located in the apicoplast. Mol Microbiol *55*, 39-53.
999 Funes, S., Davidson, E., Reyes-Prieto, A., Magallon, S., Herion, P., King, M.P., and Gonzalez-
1000 Halphen, D. (2002). A green algal apicoplast ancestor. Science *298*, 2155.
1001 Gajria, B., Bahl, A., Brestelli, J., Dommer, J., Fischer, S., Gao, X., Heiges, M., Iodice, J., Kissinger,
1002 J.C., Mackey, A.J.*, et al.* (2008). ToxoDB: an integrated *Toxoplasma gondii* database
1003 resource. Nucleic Acids Res *36*, D553-556. doi:10.1093/nar/gkm981
1004 Garrison, E.M., and Arrizabalaga, G. (2009). Disruption of a mitochondrial MutS DNA repair
1005 enzyme homologue confers drug resistance in the parasite *Toxoplasma gondii*. Mol
1006 Microbiol *72*, 425-441. doi:10.1111/j.1365-2958.2009.06655.x
1007 Gray, M.W. (2012). Mitochondrial evolution. Cold Spring Harb Perspect Biol *4*, a011403.
1008 doi:10.1101/cshperspect.a011403
1009 Gupta, A., Shah, P., Haider, A., Gupta, K., Siddiqi, M.I., Ralph, S.A., and Habib, S. (2014).
1010 Reduced ribosomes of the apicoplast and mitochondrion of *Plasmodium* spp. and
1011 predicted interactions with antibiotics. Open Biol *4*, 140045.
1012 doi:10.1098/rsob.140045
1013 Hartmann, A., Hellmund, M., Lucius, R., Voelker, D.R., and Gupta, N. (2014).
1014 Phosphatidylethanolamine synthesis in the parasite mitochondrion is required for
1015 efficient growth but dispensable for survival of *Toxoplasma gondii*. J Biol Chem *289*,
1016 6809-6824. doi:10.1074/jbc.M113.509406
1017 Hung, V., Zou, P., Rhee, H.W., Udeshi, N.D., Cracan, V., Svinkina, T., Carr, S.A., Mootha, V.K.,
1018 and Ting, A.Y. (2014). Proteomic mapping of the human mitochondrial
1019 intermembrane space in live cells via ratiometric APEX tagging. Mol Cell *55*, 332-341.
1020 doi:10.1016/j.molcel.2014.06.003
1021 Jacot, D., Waller, R.F., Soldati-Favre, D., MacPherson, D.A., and MacRae, J.I. (2015).
1022 Apicomplexan Energy Metabolism: Carbon Source Promiscuity and the Quiescence
1023 Hyperbole. Trends Parasitol *32*, 56-70. doi:10.1016/j.pt.2015.09.001
1024 Jelenska, J., Crawford, M.J., Harb, O.S., Zuther, E., Haselkorn, R., Roos, D.S., and Gornicki, P.
1025 (2001). Subcellular localization of acetyl-CoA carboxylase in the apicomplexan
1026 parasite *Toxoplasma gondii*. Proc Natl Acad Sci U S A *98*, 2723-2728.

1027 Katris, N.J., van Dooren, G.G., McMillan, P.J., Hanssen, E., Tilley, L., and Waller, R.F. (2014).
1028 The apical complex provides a regulated gateway for secretion of invasion factors in
1029 *Toxoplasma*. PLoS Pathog *10*, e1004074. doi:10.1371/journal.ppat.1004074
1030 Ke, H., Lewis, I.A., Morrisey, J.M., McLean, K.J., Ganesan, S.M., Painter, H.J., Mather, M.W.,
1031 Jacobs-Lorena, M., Llinas, M., and Vaidya, A.B. (2015). Genetic investigation of
1032 tricarboxylic acid metabolism during the *Plasmodium falciparum* life cycle. Cell Rep
1033 *11*, 164-174. doi:10.1016/j.celrep.2015.03.011
1034 Kehrer, J., Frischknecht, F., and Mair, G.R. (2016). Proteomic Analysis of the *Plasmodium*
1035 *berghei* Gametocyte Egressome and Vesicular bioID of Osmiophilic Body Proteins
1036 Identifies Merozoite TRAP-like Protein (MTRAP) as an Essential Factor for Parasite
1037 Transmission. Mol Cell Proteomics *15*, 2852-2862. doi:10.1074/mcp.M116.058263
1038 Keilhauer, E.C., Hein, M.Y., and Mann, M. (2015). Accurate protein complex retrieval by
1039 affinity enrichment mass spectrometry (AE-MS) rather than affinity purification mass
1040 spectrometry (AP-MS). Mol Cell Proteomics *14*, 120-135.
1041 doi:10.1074/mcp.M114.041012
1042 Lenaz, G., and Genova, M.L. (2010). Structure and organization of mitochondrial respiratory
1043 complexes: a new understanding of an old subject. Antioxid Redox Signal *12*, 961-
1044 1008. doi:10.1089/ars.2009.2704
1045 Limenitakis, J., Oppenheim, R.D., Creek, D.J., Foth, B.J., Barrett, M.P., and Soldati-Favre, D.
1046 (2013). The 2-methylcitrate cycle is implicated in the detoxification of propionate in
1047 *Toxoplasma gondii*. Mol Microbiol *87*, 894-908. doi:10.1111/mmi.12139
1048 MacRae, J.I., Dixon, M.W., Dearnley, M.K., Chua, H.H., Chambers, J.M., Kenny, S., Bottova, I.,
1049 Tilley, L., and McConville, M.J. (2013). Mitochondrial metabolism of sexual and
1050 asexual blood stages of the malaria parasite *Plasmodium falciparum*. BMC Biol *11*, 67.
1051 doi:10.1186/1741-7007-11-67
1052 MacRae, J.I., Sheiner, L., Nahid, A., Tonkin, C., Striepen, B., and McConville, M.J. (2012).
1053 Mitochondrial metabolism of glucose and glutamine is required for intracellular
1054 growth of *Toxoplasma gondii*. Cell Host Microbe *12*, 682-692.
1055 doi:10.1016/j.chom.2012.09.013
1056 Marechal, A., Meunier, B., Lee, D., Orengo, C., and Rich, P.R. (2012). Yeast cytochrome c
1057 oxidase: a model system to study mitochondrial forms of the haem-copper oxidase
1058 superfamily. Biochim Biophys Acta *1817*, 620-628. doi:10.1016/j.bbabio.2011.08.011
1059 Martell, J.D., Deerinck, T.J., Sancak, Y., Poulos, T.L., Mootha, V.K., Sosinsky, G.E., Ellisman,
1060 M.H., and Ting, A.Y. (2012). Engineered ascorbate peroxidase as a genetically encoded
1061 reporter for electron microscopy. Nat Biotechnol *30*, 1143-1148.
1062 doi:10.1038/nbt.2375
1063 McBride, H.M., Neuspiel, M., and Wasiak, S. (2006). Mitochondria: more than just a
1064 powerhouse. Curr Biol *16*, R551-560. doi:10.1016/j.cub.2006.06.054
1065 Messina, M., Niesman, I., Mercier, C., and Sibley, L.D. (1995). Stable DNA transformation of
1066 *Toxoplasma gondii* using phleomycin selection. Gene *165*, 213-217.
1067 Mogi, T., and Kita, K. (2009). Identification of mitochondrial Complex II subunits SDH3 and
1068 SDH4 and ATP synthase subunits a and b in *Plasmodium* spp. Mitochondrion *9*, 443-
1069 453. doi: 10.1016/j.mito.2009.08.004
1070 Mogi, T., and Kita, K. (2010). Diversity in mitochondrial metabolic pathways in parasitic
1071 protists *Plasmodium* and *Cryptosporidium*. Parasitol Int *59*, 305-312.
1072 doi:10.1016/j.parint.2010.04.005

1073 Montoya, J.G., and Liesenfeld, O. (2004). Toxoplasmosis. Lancet *363*, 1965-1976.
1074 doi:10.1016/S0140-6736(04)16412-X
1075 Moore, R.B., Obornik, M., Janouskovec, J., Chrudimsky, T., Vancova, M., Green, D.H., Wright,
1076 S.W., Davies, N.W., Bolch, C.J., Heimann, K.*, et al.* (2008). A photosynthetic alveolate
1077 closely related to apicomplexan parasites. Nature *451*, 959-963.
1078 Morales-Sainz, L., Escobar-Ramirez, A., Cruz-Torres, V., Reyes-Prieto, A., Vazquez-Acevedo,
1079 M., Lara-Martinez, R., Jimenez-Garcia, L.F., and Gonzalez-Halphen, D. (2008). The
1080 polypeptides COX2A and COX2B are essential components of the mitochondrial
1081 cytochrome c oxidase of *Toxoplasma gondii*. Biochim Biophys Acta *1777*, 202-210.
1082 doi:10.1016/j.bbabio.2007.10.013
1083 Moreno, S.N., Zhong, L., Lu, H.G., Souza, W.D., and Benchimol, M. (1998). Vacuolar-type H+-
1084 ATPase regulates cytoplasmic pH in *Toxoplasma gondii* tachyzoites. Biochem J *330 (Pt*
1085 *2)*, 853-860.
1086 Nadipuram, S.M., Kim, E.W., Vashisht, A.A., Lin, A.H., Bell, H.N., Coppens, I., Wohlschlegel,
1087 J.A., and Bradley, P.J. (2016). In Vivo Biotinylation of the *Toxoplasma* Parasitophorous
1088 Vacuole Reveals Novel Dense Granule Proteins Important for Parasite Growth and
1089 Pathogenesis. MBio *7*. doi:10.1128/mBio.00808-16
1090 Oppenheim, R.D., Creek, D.J., Macrae, J.I., Modrzynska, K.K., Pino, P., Limenitakis, J., Polonais,
1091 V., Seeber, F., Barrett, M.P., Billker, O.*, et al.* (2014). BCKDH: the missing link in
1092 apicomplexan mitochondrial metabolism is required for full virulence of *Toxoplasma*
1093 *gondii* and *Plasmodium berghei*. PLoS Pathog *10*, e1004263.
1094 doi:10.1371/journal.ppat.1004263
1095 Pankow, S., Bamberger, C., Calzolari, D., Bamberger, A., and Yates, J.R., 3rd (2016). Deep
1096 interactome profiling of membrane proteins by co-interacting protein identification
1097 technology. Nat Protoc *11*, 2515-2528. doi:10.1038/nprot.2016.140
1098 Phillips, M.A., Gujjar, R., Malmquist, N.A., White, J., El Mazouni, F., Baldwin, J., and Rathod,
1099 P.K. (2008). Triazolopyrimidine-based dihydroorotate dehydrogenase inhibitors with
1100 potent and selective activity against the malaria parasite *Plasmodium falciparum*. J
1101 Med Chem *51*, 3649-3653. doi:10.1021/jm8001026
1102 Rajendran, E., Hapuarachchi, S.V., Miller, C.M., Fairweather, S.J., Cai, Y., Smith, N.C.,
1103 Cockburn, I.A., Broer, S., Kirk, K., and van Dooren, G.G. (2017). Cationic amino acid
1104 transporters play key roles in the survival and transmission of apicomplexan
1105 parasites. Nat Commun *8*, 14455. doi:10.1038/ncomms14455
1106 Rhee, H.W., Zou, P., Udeshi, N.D., Martell, J.D., Mootha, V.K., Carr, S.A., and Ting, A.Y. (2013).
1107 Proteomic mapping of mitochondria in living cells via spatially restricted enzymatic
1108 tagging. Science *339*, 1328-1331. doi:10.1126/science.1230593
1109 Robinson, M.D., and Smyth, G.K. (2008). Small-sample estimation of negative binomial
1110 dispersion, with applications to SAGE data. Biostatistics *9*, 321-332.
1111 doi:10.1093/biostatistics/kxm030
1112 Roux, K.J., Kim, D.I., Raida, M., and Burke, B. (2012). A promiscuous biotin ligase fusion
1113 protein identifies proximal and interacting proteins in mammalian cells. J Cell Biol
1114 *196*, 801-810. doi:10.1083/jcb.201112098
1115 Sagan, L. (1967). On the origin of mitosing cells. J Theor Biol *14*, 255-274.
1116 Saito, T., Nishi, M., Lim, M.I., Wu, B., Maeda, T., Hashimoto, H., Takeuchi, T., Roos, D.S., and
1117 Asai, T. (2008). A novel GDP-dependent pyruvate kinase isozyme from *Toxoplasma*

gondii localizes to both the apicoplast and the mitochondrion. J Biol Chem *283*, 14041-14052. doi:10.1074/jbc.M709015200

Schagger, H., and Pfeiffer, K. (2000). Supercomplexes in the respiratory chains of yeast and mammalian mitochondria. EMBO J *19*, 1777-1783. doi:10.1093/emboj/19.8.1777

Seeber, F., Limenitakis, J., and Soldati-Favre, D. (2008). Apicomplexan mitochondrial metabolism: a story of gains, losses and retentions. Trends Parasitol *24*, 468-478. doi:10.1016/j.pt.2008.07.004

Sheiner, L., Demerly, J.L., Poulsen, N., Beatty, W.L., Lucas, O., Behnke, M.S., White, M.W., and Striepen, B. (2011). A systematic screen to discover and analyze apicoplast proteins identifies a conserved and essential protein import factor. PLoS Pathog *7*, e1002392. doi:10.1371/journal.ppat.1002392

Shen, B., Brown, K.M., Lee, T.D., and Sibley, L.D. (2014). Efficient gene disruption in diverse strains of *Toxoplasma gondii* using CRISPR/CAS9. MBio *5*, e01114-01114. doi:10.1128/mBio.01114-14

Sickmann, A., Reinders, J., Wagner, Y., Joppich, C., Zahedi, R., Meyer, H.E., Schonfisch, B., Perschil, I., Chacinska, A., Guiard, B.*, et al.* (2003). The proteome of *Saccharomyces cerevisiae* mitochondria. Proc Natl Acad Sci U S A *100*, 13207-13212. doi:10.1073/pnas.2135385100

Sidik, S.M., Huet, D., Ganesan, S.M., Huynh, M.H., Wang, T., Nasamu, A.S., Thiru, P., Saeij, J.P., Carruthers, V.B., Niles, J.C.*, et al.* (2016). A Genome-wide CRISPR Screen in *Toxoplasma* Identifies Essential Apicomplexan Genes. Cell *166*, 1423-1435. doi:10.1016/j.cell.2016.08.019

Srivastava, I.K., Morrisey, J.M., Darrouzet, E., Daldal, F., and Vaidya, A.B. (1999). Resistance mutations reveal the atovaquone-binding domain of cytochrome *b* in malaria parasites. Mol Microbiol *33*, 704-711.

Striepen, B., and Soldati, D. (2007). Genetic manipulation of *Toxoplasma gondii*. In *Toxoplasma gondii* The Model Apicomplexan - Perspectives and Methods, L.D. Weiss, and K. Kim, eds. (London: Elsevier), pp. 391-415.

Sturm, A., Mollard, V., Cozijnsen, A., Goodman, C.D., and McFadden, G.I. (2015). Mitochondrial ATP synthase is dispensable in blood-stage *Plasmodium berghei* rodent malaria but essential in the mosquito phase. Proc Natl Acad Sci U S A *112*, 10216-10223. doi:10.1073/pnas.1423959112

Tonkin, C.J., van Dooren, G.G., Spurck, T.P., Struck, N.S., Good, R., Handman, E., Cowman, A.F., and McFadden, G.I. (2004). Localization of organellar proteins in *Plasmodium falciparum* using a novel set of transfection vectors and a new immunofluorescence fixation method. Mol Biochem Parasitol *137*, 13-21.

Toursel, C., Dzierszinski, F., Bernigaud, A., Mortuaire, M., and Tomavo, S. (2000). Molecular cloning, organellar targeting and developmental expression of mitochondrial chaperone HSP60 in *Toxoplasma gondii*. Mol Biochem Parasitol *111*, 319-332.

Tsukihara, T., Aoyama, H., Yamashita, E., Tomizaki, T., Yamaguchi, H., Shinzawa-Itoh, K., Nakashima, R., Yaono, R., and Yoshikawa, S. (1996). The whole structure of the 13-subunit oxidized cytochrome c oxidase at 2.8 A. Science *272*, 1136-1144.

van Dooren, G.G., Reiff, S.B., Tomova, C., Meissner, M., Humbel, B.M., and Striepen, B. (2009). A novel dynamin-related protein has been recruited for apicoplast fission in *Toxoplasma gondii*. Curr Biol *19*, 267-276. doi:10.1016/j.cub.2008.12.048

van Dooren, G.G., Stimmler, L.M., and McFadden, G.I. (2006). Metabolic maps and functions of the *Plasmodium* mitochondrion. FEMS Microbiol Rev *30*, 596-630. doi:10.1111/j.1574-6976.2006.00027.x

van Dooren, G.G., Tomova, C., Agrawal, S., Humbel, B.M., and Striepen, B. (2008). *Toxoplasma gondii* Tic20 is essential for apicoplast protein import. Proc Natl Acad Sci U S A *105*, 13574-13579.

van Dooren, G.G., Yeoh, L.M., Striepen, B., and McFadden, G.I. (2016). The Import of Proteins into the Mitochondrion of *Toxoplasma gondii*. J Biol Chem *291*, 19335-19350. doi:10.1074/jbc.M116.725069

Zikova, A., Hampl, V., Paris, Z., Tyc, J., and Lukes, J. (2016). Aerobic mitochondria of parasitic protists: Diverse genomes and complex functions. Mol Biochem Parasitol *209*, 46-57. doi:10.1016/j.molbiopara.2016.02.007

Zimmermann, L., Stephens, A., Nam, S.Z., Rau, D., Kubler, J., Lozajic, M., Gabler, F., Soding, J., Lupas, A.N., and Alva, V. (2017). A Completely Reimplemented MPI Bioinformatics Toolkit with a New HHpred Server at its Core. J Mol Biol. doi:10.1016/j.jmb.2017.12.007

1181 **FIGURE LEGENDS**

1182

1183 **Figure 1.** Biotinylation of mitochondrial matrix proteins in *T. gondii* parasites expressing
1184 mtAPEX and mtBirA*. (A-B) Immunofluorescence assays of parasites expressing c-myc-tagged,
1185 mitochondrially-targeted APEX (A) and BirA* (B), labelled with anti-c-myc (green) and the
1186 mitochondrial marker *Tg*Tom40 (red). Scale bars are 2 µm. (C-D) Western blots of parasites
1187 expressing c-myc-tagged, mitochondrially-targeted APEX (C) and BirA* (D), labelled with anti-
1188 c-myc. (E) Oregon Green-conjugated avidin (Avidin-OG) labelling of *T. gondii* parasites
1189 expressing mtAPEX, and cultured in the absence (top) or presence (bottom) of biotin-phenol and
1190 H_2O_2. Biotinylated proteins are labelled in green. (F) Avidin-OG labelling of *T. gondii* parasites
1191 expressing mtBirA*, and cultured in the absence (top) or presence (bottom) of biotin.
1192 Biotinylated proteins are labelled in green. Scale bars are 2 µm. (G) Neutravidin-HRP protein
1193 blot of WT, mtBirA* or mtAPEX parasites cultured in the presence of biotin or biotin-phenol.
1194 (H) Western blots of the mitochondrial matrix marker mtHsp60 and the mitochondrial
1195 intermembrane space marker cyt *c* in WT, mtBirA* or mtAPEX parasites cultured in the
1196 presence of biotin (lanes 1-4) or biotin-phenol (lanes 5-8). Parasites were either harvested
1197 following treatment to yield the total (T) protein fraction, or biotinylated proteins were purified
1198 on a streptavidin-agarose column to yield the bound (B) fraction.

1199

1200 **Figure 2.** The mitochondrial proteome of *T. gondii*. (A-B) Volcano plots showing the $\log_2$
1201 protein ratios vs –log10 *p* values of biotinylated proteins in WT compared to mtAPEX
1202 (WT/APEX) samples (A) and in WT compared to mtBirA* samples (WT/BirA*) (B) following
1203 the quantitative pipeline analysis. Proteins were deemed to be enriched in the mitochondrion if

the $\log_2$ fold change in protein expression was $\geq$-2.5 and the *p* value ≤ 0.001 (red). (C) Venn diagram of the mtAPEX and mtBirA* proteomes. 161 proteins were identified in both proteomes, while 52 were unique to the mtAPEX proteome and 208 unique to the mtBirA* proteome. (D) Metabolic map of expected mitochondrial proteins (circles), showing proteins present (blue) and absent (yellow) from the *T. gondii* mitochondrial proteome. Black arrows represent the flow of metabolites through metabolic pathways in the mitochondrion, and blue arrows depict the flow of ions, minerals or metabolic pathway products.

Figure 2 – figure supplement 1. Analysis of putative mitochondrial targeting peptides in the *T. gondii* mitochondrial proteome. Pie chart depicting mitochondrial targeting peptide predictions of the *T. gondii* mitochondrial proteome using MitoProt II. Proteins with high (>0.9; blue), medium (0.5-0.9; aqua) and low (<0.5; pink) prediction scores are shown.

Figure 3. The localization of novel proteins from the *T. gondii* mitochondrial proteome. (A-AA) Proteins with no previously determined localization in *T. gondii* were selected from the mitochondrial proteome, and the corresponding gene was tagged at the 3'-terminus of the open reading frame with a HA tag. Immunofluorescence assays depict HA-tagged proteins (green) co-labelled with the mitochondrial marker *Tg*Tom40 (red). The http://toxodb.org gene identification number is depicted for every gene that was tagged.

Figure 4. Orthology analyses of proteins from the *T. gondii* mitochondrial proteome reveal that many mitochondrial proteins are restricted to *T. gondii* and related organisms, and that most are important for parasite survival. (A) Bar graph depicting the percentage of orthologs from the

mitochondrial proteome of *T. gondii* (*Tg*) found in *P. falciparum* (*Pf*), *B. bovis* (*Bb*), *C. parvum* (*Cp*) and *V. brassicaformis* (*Vb*). Phenotype scores are indicated with shading, and reveal that most ortholog groups in each category are important or critical for tachyzoite growth. (B-C) Venn diagram depicting ortholog groupings from the mitochondrial proteome of *T. gondii* compared to (B) non-coccidian apicomplexans, chromerids and eukaryotes, or (C) non-coccidian apicomplexans, chromerids and animals. (D) Bar graph depicting distribution of phenotype scores in genes belonging to ortholog groups found only in *T. gondii* and other coccidians (*Tg* only), in *T. gondii*, non-coccidian apicomplexans and chromerids (*Tg*+Api+Chr), and in *T. gondii*, non-coccidian apicomplexans, chromerids and animals (*Tg*+Api+Chr+Api). In (A) and (D), genes with phenotype scores of ≥-2 were considered dispensable, -2 to -4 were considered important, and ≤-4 were considered critical.

Figure 5. *Tg*ApiCox25 is important for parasite growth and mitochondrial O_2 consumption. (A) Western blot of proteins extracted from r*Tg*ApiCox25-HA parasites grown in the absence of ATc, or in ATc for 1-3 days, and detected using anti-HA antibodies (top) and anti-*Tg*Tom40 (as a loading control; bottom). (B) Plaque assays measuring growth of WT, r*Tg*ApiCox25 and complemented c*Tg*ApiCox25-HA/r*Tg*ApiCox25 parasites cultured in the absence (top) or presence (bottom) of ATc. Assays are from a single experiment and are representative of 3 independent experiments. (C) Quantification of plaque size from WT, r*Tg*ApiCox25 and complemented c*Tg*ApiCox25-HA/r*Tg*ApiCox25 parasites grown in the absence or presence of ATc for 9 days. Box and whisker plots depict the median plaque size (centre line), the 25th and 75th percentiles (box) and the 5th and 95th percentiles (lines). Data are from 30 plaques per flask from a single experiment, except in the case of the r*Tg*ApiCox25 strain, where only 18 plaques

were discernible. (D) Basal mitochondrial oxygen consumption rates (mOCR) in WT parasites grown in the absence of ATc or in the presence of ATc for 3 days (orange), and r*Tg*ApiCox25 parasites grown in the absence of ATc, or in the presence of ATc for 1-3 days (blue). A linear mixed-effects model was fitted to the data, and the values depict the mean ± s.e.m. from three independent experiments (a one-way ANOVA followed by Tukey's multiple pairwise comparison test was performed. Relevant *p* values are shown). (E) Basal mOCR plotted against basal extracellular acidification rate (ECAR) of WT cells grown in the absence of ATc, the presence of cycloheximide (CHX) for 1 day, or the presence of ATc for 3 days, and r*Tg*ApiCox25 parasites grown in the absence of ATc or presence of ATc for 1-3 days (mean ± s.e.m. of the linear mixed-effects model described above; n = 3).

Figure 5 – figure supplement 1. Generating an ATc-regulated promoter replacement strain of *Tg*ApiCox25. (A) Diagram depicting the promoter replacement strategy to generated ATc-regulated *Tg*ApiCox25. A single guide RNA (sgRNA) was designed to target the *T. gondii* genome near the start codon of *Tg*ApiCox25, and mediate a double stranded break at the target site. A plasmid containing the sgRNA and GFP-tagged Cas9 endonuclease was co-transfected into *T. gondii* parasites with a PCR product encoding the ATc regulated 't7s4' promoter, which contains 7 copies of the Tet operon and a Sag4 minimal promoter, flanked by 50 bp of sequence homologous to the regions immediately up- and down-stream of the *Tg*ApiCox25 start codon. The PCR product also contain a 'spacer' region that separates the regulatable promoter from the native promoter of *Tg*ApiCox25 gene to enable sufficient regulation. The parasite's homologous repair pathway will mediate integration of the PCR product into the *Tg*ApiCox25 locus. The '*Tg*ApiCox25 fwd', '*Tg*ApiCox25 rvs' and 't7s4 fwd' primers were used in screening parasite

clones for successful integration of the regulatable promoter at the target site. (B-C) PCR screening analysis using genomic DNA extracted from parasite clones to identify clones that had successfully integrated the promoter. (B) Screening using the *Tg*ApiCox25 fwd and rvs primers. This will amplify a product of 1,064 bp if the locus is unmodified, and a product of 2,991 bp if the ATc-regulatable promoter has integrated successfully. (C) Screening using the *Tg*ApiCox25 rvs and t7s4 fwd primers. This will amplify a product of 928 bp if the ATc-regulatable promoter has integrated successfully. The analyses in B and C revealed that clone 3 had successfully integrated the ATc-regulatable promoter.

Figure 5 – figure supplement 2. Knockdown of *Tg*ApiCox25 leads to defects in maximal mOCR. Maximal mOCR, comprising of the sum of the basal mOCR (colored) and the spare capacity (white), of TATi/Δ*ku80* (WT) parasites grown in the absence of ATc or in the presence of ATc for 3 days (orange), and r*Tg*ApiCox25 cells grown in the absence of ATc, or in the presence of ATc for 1-3 days (blue). A linear mixed-effects model was fitted to the data, which are depicted as the mean ± s.e.m. from three independent experiments (a one-way ANOVA followed by Tukey's multiple pairwise comparison test was performed. Relevant *p* values are shown).

Figure 5 – figure supplement 3. Defects in OCR upon *Tg*ApiCox25 knockdown are not the result of general defects in mitochondrial morphology or parasite viability. (A) Immunofluorescence assays assessing mitochondrial morphology in r*Tg*ApiCox25 parasites grown in the absence of ATc (top) or in the presence of ATc for 3 days (bottom). Mitochondria were labelled using antibodies against *Tg*Tom40 (red). Images are representative of 100 four-cell

vacuoles examined in two independent experiments. The scale bar is 2 μm. (B) Plaque assays of r*Tg*ApiCox25 parasites grown for 9 days in the absence (left) or presence (right) of ATc. r*Tg*ApiCox25 parasites were not preincubated in ATc (no ATc preinc; top) or pre-incubated in ATc for 3 days (3d + ATc preinc; bottom) before commencing the experiment. Plaque assays are from a single experiment, representative of 3 independent experiments.

Figure 6. *Tg*ApiCox25 is a component of the cytochrome *c* oxidase complex, and important for complex integrity. (A) Western blot of proteins extracted from *Tg*ApiCox25-HA parasites, separated by blue native-PAGE, and detected with anti-HA antibodies. (B) Western blot of proteins extracted from *Tg*ApiCox25-HA parasites, separated by SDS-PAGE, and detected with anti-HA antibodies. (C) Volcano plot showing the $\log_2$ fold change vs $-\log_{10} p$ values of proteins purified from *Tg*ApiCox25-HA vs *Tg*Tom40-HA parasites using anti-HA immunoprecipitations and detected by mass spectrometry. Only proteins detected in each of the three independent experiments for both parasite lines are depicted. Proteins enriched in the *Tg*ApiCox25-HA samples ($p < 0.05$; $\log_2$ fold change >5) have been coded according to whether they are orthologous to canonical cytochrome *c* oxidase subunits (green triangles), or restricted to the apicomplexan lineage (blue circle; ApiCox subunits). *Tg*ApiCox25 is also depicted (red diamond).

Figure 6 – figure supplement 1. Immunopurification of the *Tg*ApiCox25 and *Tg*Tom40 protein complexes. (A-B) Western blots of proteins extracted from parasites expressing *Tg*ApiCox25-HA (A) or *Tg*Tom40-HA (B). Extracts include samples before immunoprecipitation (Total), samples that did not bind to the anti-HA beads (Unbound), and samples that bound to the anti-

HA beads (Bound). Samples were probed with anti-HA (top) and anti-*Tg*Tom40 (bottom) antibodies. Immunoprecipitions are representative of three independent experiments. Bound fractions from each experiment were subjected to mass spectrometry-based protein identification.

Figure 7. *Tg*ApiCox25 is a component of *T. gondii* cytochrome *c* oxidase and important for complex integrity. (A) Anti-FLAG western blot of proteins from the *Tg*Cox2a-FLAG/*Tg*ApiCox25-HA strain separated by blue native-PAGE. (B) Western blots of proteins extracted from the *Tg*Cox2a-FLAG/ *Tg*ApiCox25-HA strain and subjected to immunoprecipitation using anti-HA (anti-HA IP) or anti-FLAG (anti-FLAG IP) antibody-coupled beads. Extracts include samples before immunoprecipitation (Total), samples that did not bind to the anti-HA or anti-FLAG beads (Unbound), and samples that bound to the anti-HA or anti-FLAG beads (Bound). Samples were probed with anti-HA to detect *Tg*ApiCox25-HA, anti-FLAG to detect *Tg*Cox2a-FLAG, anti-AtpB to detect the β-subunit of *T. gondii* ATP synthase, and anti-*Tg*Tom40. (C) Anti-HA (left) and anti-FLAG (right) western blots of proteins from the *Tg*ApiCox25-FLAG/*Tg*ApiCox30-HA strain separated by blue native-PAGE. (D) Western blots of proteins extracted from the *Tg*ApiCox25-FLAG/*Tg*ApiCox30-HA strain and subjected to immunoprecipitation using anti-HA (anti-HA IP) or anti-FLAG (anti-FLAG IP) antibody-coupled beads. Extracts include samples before immunoprecipitation (Total), samples that did not bind to the anti-HA or anti-FLAG beads (Unbound), and samples that bound to the anti-HA or anti-FLAG beads (Bound). Samples were probed with anti-HA to detect *Tg*ApiCox30-HA, anti-FLAG to detect *Tg*ApiCox25-FLAG, anti-AtpB, and anti-*Tg*Tom40. (E) Western blot of proteins extracted from r*Tg*ApiCox25-HA/*Tg*Cox2a-FLAG parasites grown in

the absence of ATc, or in ATc for 1-3 days, separated by SDS-PAGE and detected using anti-HA (top), anti-FLAG (middle) and anti-*Tg*Tom40 (as a loading control; bottom). (F) Western blot of proteins extracted from *Tg*Cox2a-FLAG/r*Tg*ApiCox25-HA parasites grown in the absence of ATc, or in ATc for 1-3 days, separated by blue native-PAGE, and detected using anti-FLAG antibodies.

Figure 7 – figure supplement 1. Generating FLAG tagged *Tg*Cox2a and *Tg*ApiCox25 strains. (A) Diagram depicting the 3' replacement strategy to generate FLAG-tagged *Tg*Cox2a. A single guide RNA (sgRNA) was designed to target the *T. gondii* genome near the stop codon of *Tg*Cox2a, and mediate a double stranded break at the target site. A plasmid containing the sgRNA and GFP-tagged Cas9 endonuclease was co-transfected into *T. gondii* parasites with a PCR product encoding a FLAG epitope tag flanked by 50 bp of sequence homologous to the regions immediately up- and down-stream of the *Tg*Cox2a stop codon. The parasite's homologous repair pathway will mediate integration of the PCR product into the *Tg*Cox2a locus. Forward and reverse primers were used to screen parasite clones for successful integration of the FLAG tag at the target site, yielding a 260 bp product in the native locus and a 361 bp product in the modified locus. (B) PCR screening analysis using genomic DNA extracted from putative *Tg*Cox2a-FLAG/*Tg*ApiCox25-HA parasites (clones 1-10) and *Tg*Cox2a-FLAG/r*Tg*ApiCox25-HA parasites (clones 11-12). Clones 1-5 and 7-12 yielded PCR products that indicated that these clones had been successfully modified. (C) Diagram depicting the 3' replacement strategy to generate FLAG-tagged *Tg*ApiCox25. A single guide RNA (sgRNA) was designed to target the *T. gondii* genome near the stop codon of *Tg*ApiCox25, and mediate a double stranded break at the target site. A plasmid containing the sgRNA and GFP-tagged Cas9 endonuclease was co-

transfected into *T. gondii* parasites with a PCR product encoding a FLAG epitope tag flanked by 50 bp of sequence homologous to the regions immediately up- and down-stream of the *Tg*ApiCox25 stop codon. The parasite's homologous repair pathway will mediate integration of the PCR product into the *Tg*ApiCox25 locus. Forward and reverse primers were used to screen parasite clones for successful integration of the FLAG tag at the target site, yielding a 385 bp product in the native locus and a 492 bp product in the modified locus. (B) PCR screening analysis using genomic DNA extracted from putative *Tg*ApiCox25-FLAG/*Tg*ApiCox30-HA parasites. Clones 1, 5-7 yielded PCR products that indicated that these clones had been successfully modified.

SUPPLEMENTARY FILES

Supplementary File 1. List of genes encoding putative *T. gondii* mitochondrial proteins. **Tab 1.** List of peptides identified in the APEX and BirA* proteomic analyses. Included are the ToxoDB accession numbers, the identified peptide, the experiment in which the peptide was identified, and the charge, m/z ratio, mass error, posterior error probability, score, delta score and intensity of each peptide from each experiment. **Tab 2.** List of proteins identified in the RH control and mtAPEX proteomes, including the ToxoDB accession numbers, the $\log_2$ protein ratios, *p* value, and unique sequence counts. **Tab 3.** List of proteins identified in the RH control and mtBirA* proteomes, including the ToxoDB accession numbers, the $\log_2$ protein ratios, *p* value, and unique sequence counts. **Tab 4.** Summary of putative mitochondrial proteins identified in this study. The summary includes the ToxoDB accession numbers and annotation of proteins identified

from the combined list (colums A and B), proteins identified in both lists (columns D and E), and proteins identified in the mtAPEX proteome (columns G and H) or mtBirA* (columns J and K) proteomes only. Proteins highlighted in green were demonstrated by this study to localise to the mitochondrion, while those highlighted in red did not localise to the mitochondrion. **Tab 5.** Annotated protein list of the *T. gondii* mitochondrial proteome, noting the ToxoDB accession number of the corresponding gene, the protein annotation, mean phenotype score, molecular mass, number of transmembrane domains, amino acid sequence, MitoProt II prediction score, the ortholog grouping, and the accession number of orthologous genes in *P. falciparum*, *C. parvum*, *B. bovis*, and *V. brassicaformis* based on reciprocal BLAST searches. **Tab 6**. Summary of the OrthoMCL analysis of the *T. gondii* mitochondrial proteome, depicting the gene annotation, mean phenotype score, and the relevant orthology grouping.

Supplementary File 2. Summary of metabolic pathway enrichment in the *T. gondii* mitochondrial proteome. Metabolic pathway enrichment analysis was performed using the Metabolic Pathway search tool on ToxoDB (http://toxodb.org), using a p value cut-off of <0.05.

Supplementary File 3. True positives and false negatives identified from the *T. gondii* mitochondrial proteome. List of proteins identified in the *T. gondii* mitochondrial proteome that previous studies have demonstrated or predicted to localize to the mitochondrion, and proteins that previous studies have demonstrated do not localize to the mitochondrion. Color coding: dark green, predicted mitochondrial protein present in proteome; pink, predicted mitochondrial protein absent from proteome; light green, predicted non-mitochondrial protein absent from proteome.

Supplementary File 4. List of primers used in localization studies. 3' fragments of target genes (ToxoDB gene ID) were amplified using the listed forward and reverse primers. The resulting PCR product was digested and ligated into the vector pgCH as outlined in the cloning strategy. The final vector was linearized with the indicated restriction enzyme before transfection.

Supplementary File 5. Tab 1. List of proteins identified in the *Tg*ApiCox25 and *Tg*Tom40 immunoprecipitations. Included is a description of each identified protein, the UniProt accession number, the predicted molecular mass, the fold change, the normalized total precursor intensity for each biological replicate, and the Cox or ApiCox designation of the identified protein. **Tab 2.** A list of the log fold change (logFC) and *p* values calculated for each protein identified in all replicates of the *Tg*ApiCox25 and *Tg*Tom40 immunoprecipitations following EdgeR analysis.

Source Code File 1. R script used in the analysis of the Seahorse XFe96 data.

Source Code File 2. R script used in the analysis of proteomic data from the *Tg*ApiCox25 and *Tg*Tom40 immunoprecipitations.

Table 1. Summary of the features of proteins identified in proteomic analysis of the *Tg*ApiCox25 complex. Similarity searches were performed using HMMER (https://www.ebi.ac.uk/Tools/hmmer/). The accession numbers listed were derived from http://EuPathDB.org (apicomplexan and chromerid species) or www.ncbi.nlm.nih.gov (all others). Abbreviations: *Plasmodium falciparum (Pf), Cryptosporidium parvum (Cp), Vitrella brassicaformis (Vb), Saccharomyces cerevisiae (Sc), Homo sapiens (Hs), Arabidopsis thaliana (At).*

ToxoDB gene ID (http://toxodb.org)	**Protein Annotation**	**Mitochondrial proteome** (this study)	**Phenotype Score** (Sidik *et al.*, 2016)	**Similarity Search** (E-value)					
				Pf (Apicomplexan)	*Cp* (Apicomplexan)	*Vb* (Chromerid)	*Sc* (Fungi)	*Hs* (Animal)	*At* (Plant)
TGGT1_264040	Hypothetical protein (***Tg*ApiCox25**)	✓	-2.54	Conserved unknown protein PF3D7_1464000.1 ($2.4e^{-53}$)	x	Hypothetical Protein Vbra_12326.t1 ($5.2e^{-29}$)	x	x	x
TGGT1_265370	Hypothetical protein (***Tg*ApiCox16**)	✓	1.56	x	x	x	x	x	x
TGGT1_209260	Putative cytochrome *c* oxidase subunit (***Tg*Cox5b**)	✓	-3.07	Putative COX5B PF3D7_0927800.1 ($4.3e^{-101}$)	x	COX5B-2 Vbra_9355.t1 ($1.6e^{-92}$)	Cox4p P04037 (0.32)	Cox5B NP_001853.2 (0.05)	COX5b At1g80230 ($2.1e^{-08}$)
TGGT1_221510	Hypothetical protein (***Tg*ApiCox18**)	✓	-3.28	Conserved unknown protein PF3D7_0523300.1 ($1.5e^{-48}$)	x	Hypothetical Protein Vbra_21271.t1 ($5.2e^{-45}$)	x	x	x
TGGT1_262640	Hypothetical protein (***Tg*ApiCox23**)	✓	-3.49	Conserved unknown protein PF3D7_0708700.1 ($3.1e^{-64}$)	x	Hypothetical Protein Vbra_3012.t1 ($2.4e^{-53}$)	x	x	x
TGGT1_297810	Hypothetical protein (***Tg*ApiCox30**)	✓	-3.64	Conserved unknown protein PF3D7_0915700.1 ($1.2e^{-46}$)	x	Hypothetical Protein Vbra_17445.t1 ($6.7e^{-33}$)	x	x	x
TGGT1_247770	Hypothetical protein (***Tg*ApiCox19**)	✓	-2.61	Conserved unknown protein PF3D7_1402200.1 ($1.2e^{-34}$)	x	Hypothetical Protein Vbra_2065.t1 ($1.7e^{-27}$)	x	x	x
TGGT1_229920	Hypothetical protein (***Tg*ApiCox35**)	✓	-3.84	Conserved unknown protein PF3D7_0306500.1 ($1.5e^{-90}$)	x	Hypothetical Protein Vbra_6819.t1 ($1.6e^{-73}$)	x	x	x
TGGT1_306670	Hypothetical protein (***Tg*ApiCox26**)	✓	-3.68	Conserved unknown protein PF3D7_1439600.1 ($2.6e^{-43}$)	x	Hypothetical Protein Vbra_888.t1 ($1.2e^{-36}$)	x	x	x
TGGT1_226590	Putative cytochrome *c* oxidase subunit (***Tg*Cox2a**)	✓	-3.80	Cytochrome c oxidase subunit 2 PF3D7_1361700.1 ($4.9e^{-58}$)	x	Cytochrome c oxidase subunit 2 Vbra_8641.t1 ($3.6e^{-33}$)	Cox2 P00410 ($2.6e^{-06}$)	Cox2 P00403 (0.0004)	Cox2 P93285 ($3.3e^{-06}$)
TGGT1_310470	Putative cytochrome *c* oxidase subunit (***Tg*Cox2b**)	✓	-4.18	Cytochrome c oxidase subunit 2 PF3D7_1430900.1 ($7.6e^{-75}$)	x	Cytochrome c oxidase subunit 2 Vbra_14923.t1 ($4.2e^{-7}$)	Cox2 P00410 ($4.3e^{-31}$)	Cox2 P00403 ($9.2e^{-29}$)	Cox2 P93285 ($3.8e^{-37}$)
TGGT1_286530	Hypothetical protein (***Tg*ApiCox24**)	✓	-2.82	Conserved unknown protein PF3D7_1362000.1 ($6.0e^{-45}$)	x	Hypothetical Protein Vbra_10089.t1 ($1.2e^{-11}$)	x	x	x

Figure 1

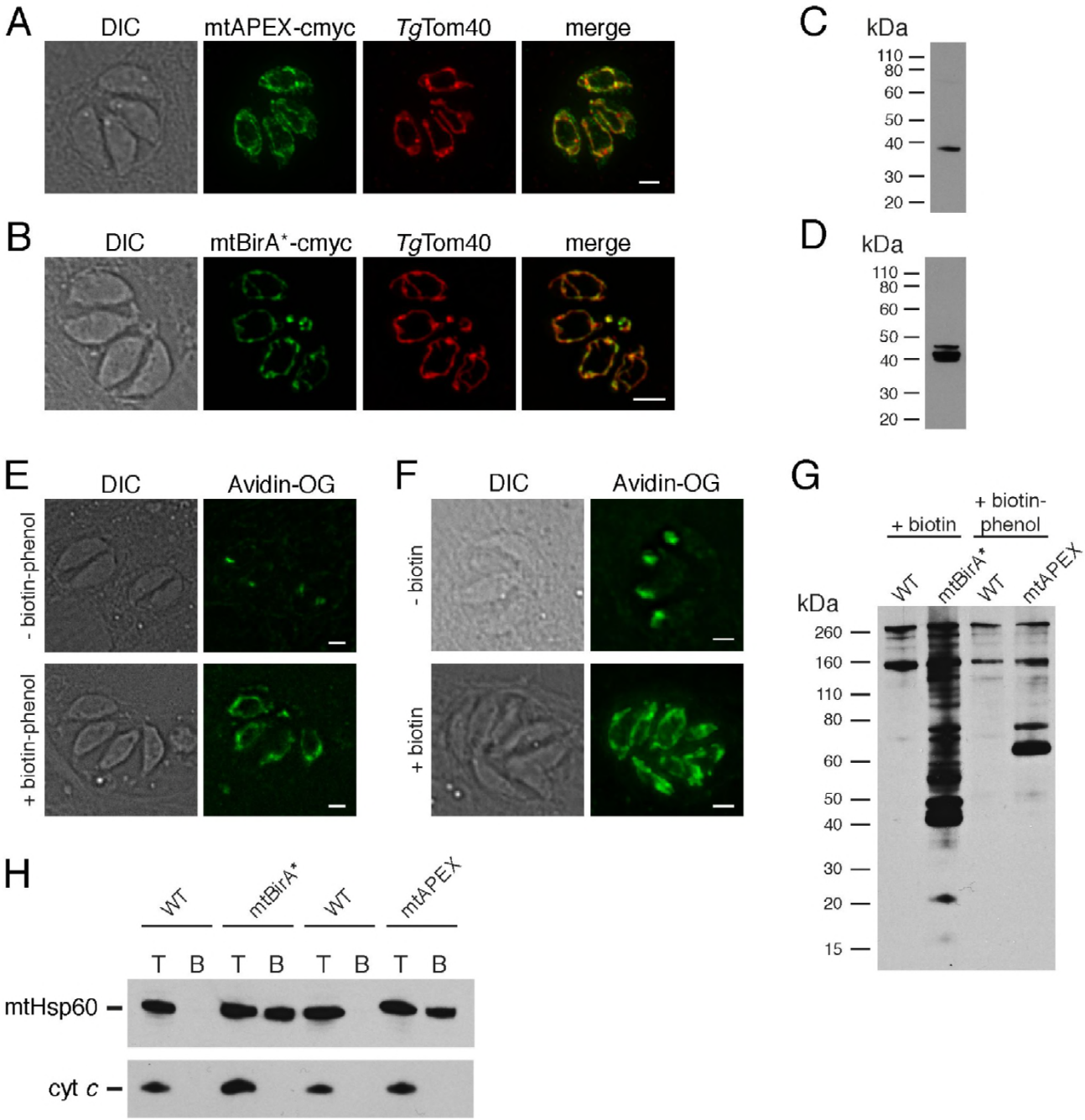
A
DIC
mtAPEX-cmyc
TgTom40
merge
B
DIC
mtBirA*-cmyc
TgTom40
merge
C
kDa
110
80
60
50
40
30
20
D
kDa
110
80
60
50
40
30
20
E
DIC
Avidin-OG
- biotin-phenol
+ biotin-phenol
F
DIC
Avidin-OG
- biotin
+ biotin
G
+ biotin
+ biotin-phenol
WT
mtBirA*
WT
mtAPEX
kDa
260
160
110
80
60
50
40
30
20
15
H
WT
mtBirA*
WT
mtAPEX
T B T B T B T B
mtHsp60
cyt c

Figure 2

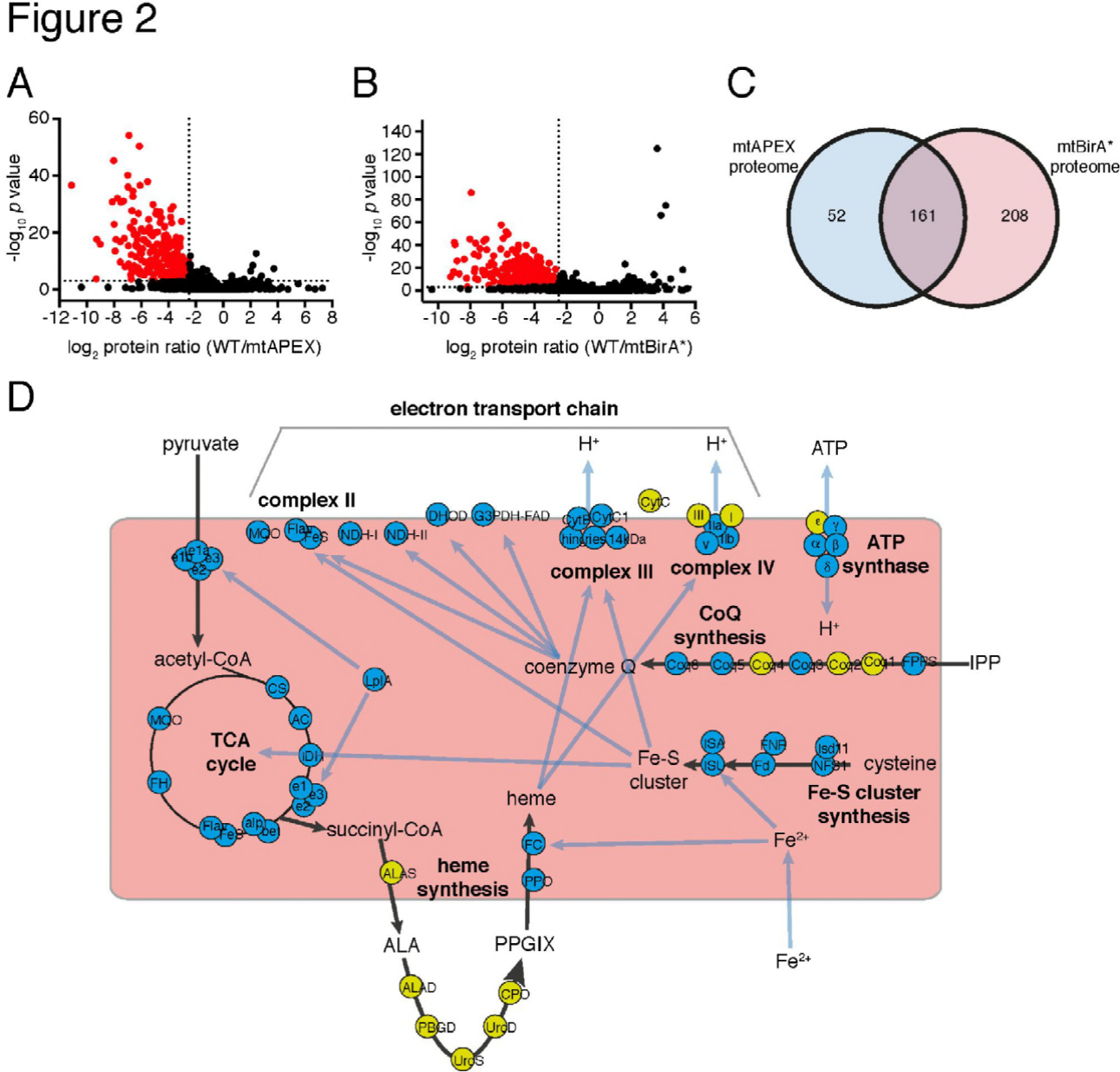
A
B
C
D
-log10 p value
log2 protein ratio (WT/mtAPEX)
log2 protein ratio (WT/mtBirA*)
mtAPEX proteome
mtBirA* proteome
52
161
208
electron transport chain
pyruvate
H+
ATP
complex II
complex III
complex IV
ATP synthase
CoQ synthesis
coenzyme Q
IPP
acetyl-CoA
TCA cycle
Fe-S cluster
cysteine
Fe-S cluster synthesis
heme
heme synthesis
succinyl-CoA
ALA
PPGIX
Fe2+

Figure 2 - figure supplement 1

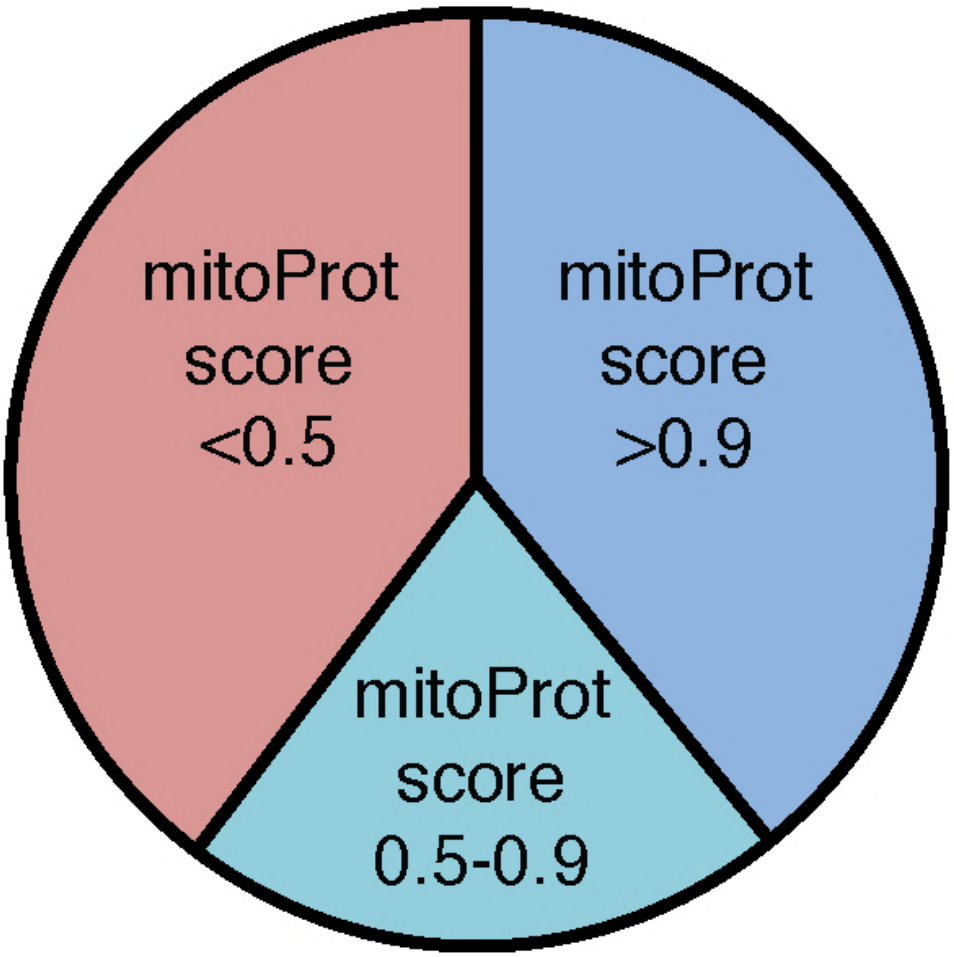

Figure 3

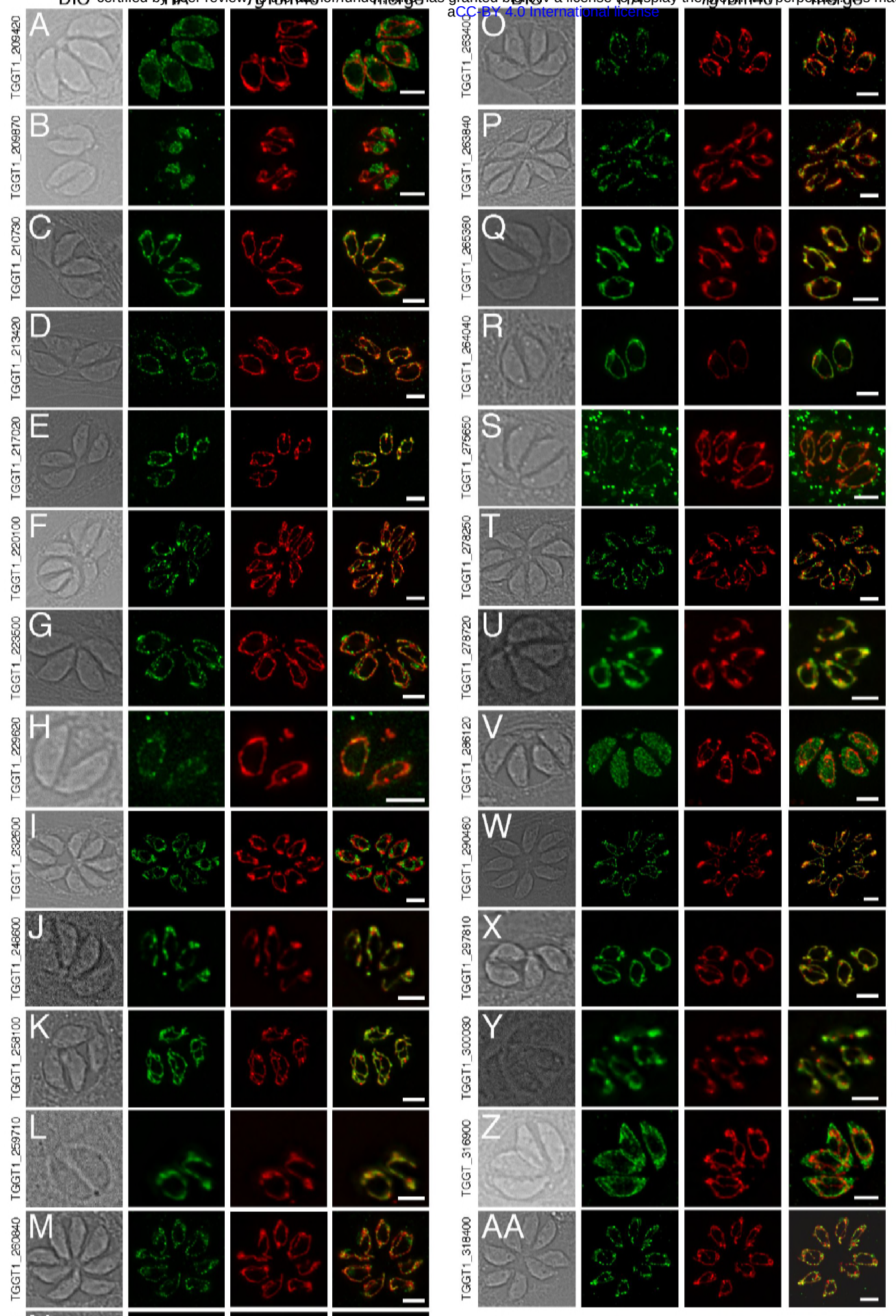

Figure 4

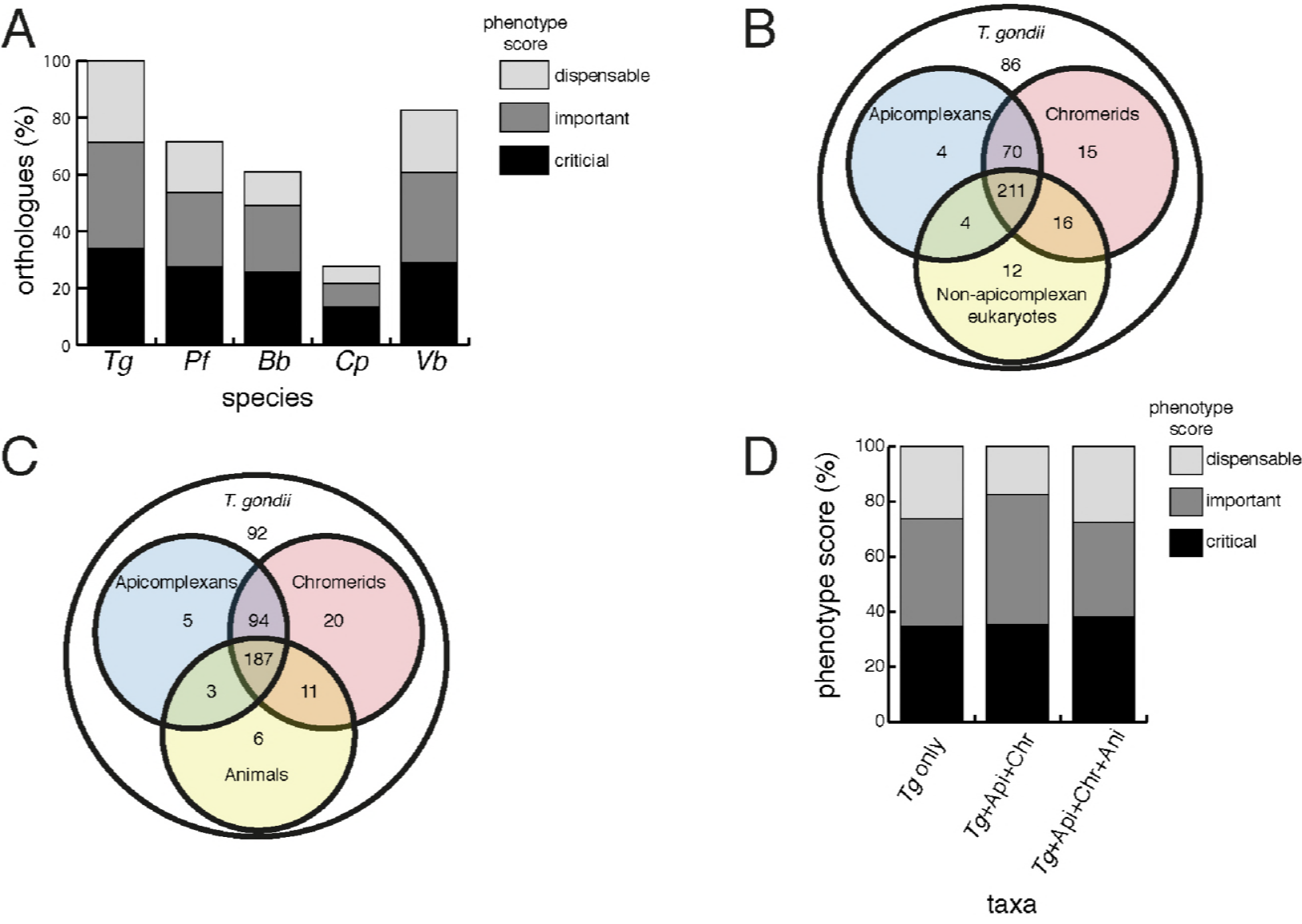

Figure 5

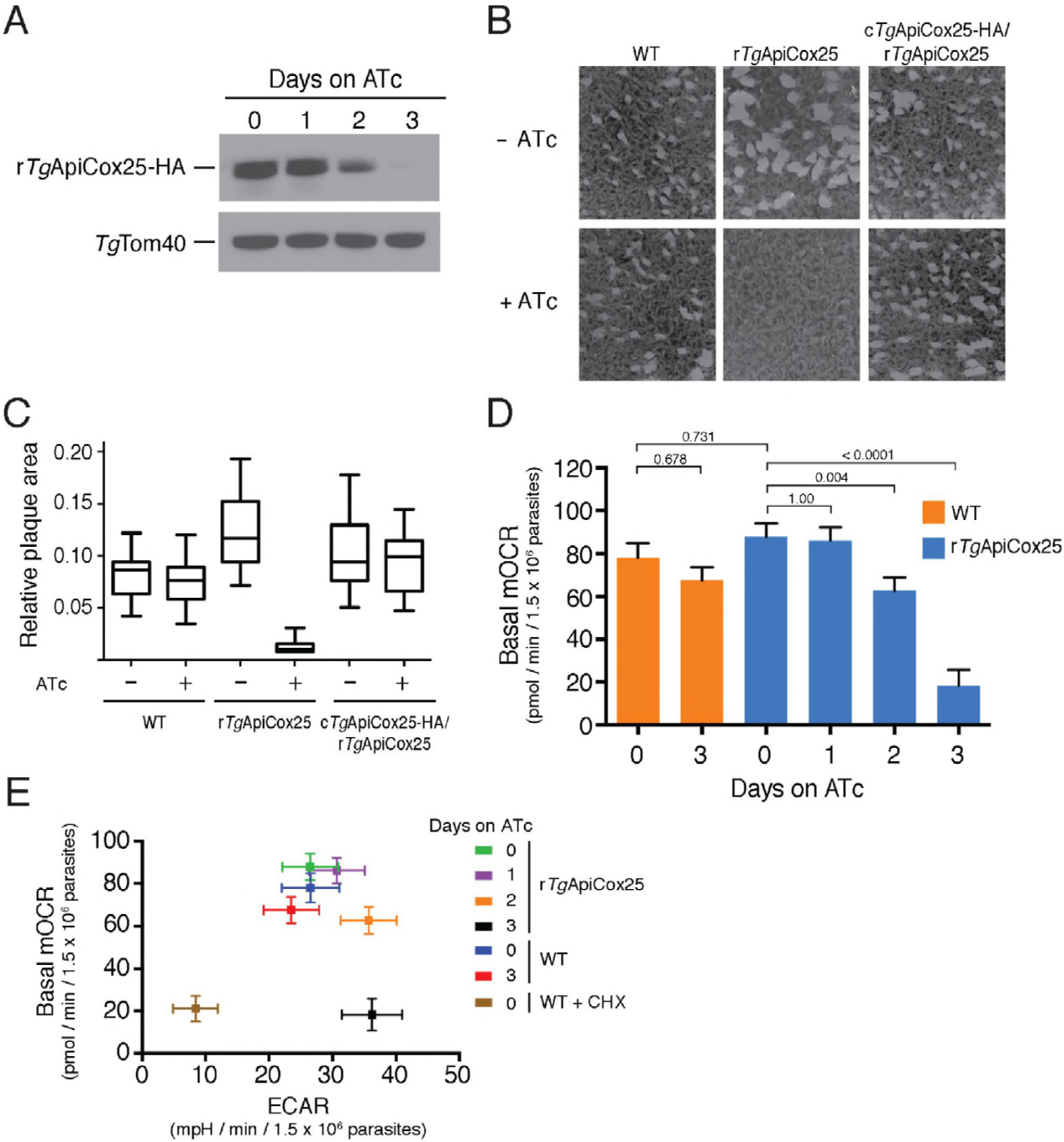
A
Days on ATc
0 1 2 3
rTgApiCox25-HA
TgTom40
B
WT
rTgApiCox25
cTgApiCox25-HA/
rTgApiCox25
- ATc
+ ATc
C
Relative plaque area
0.20
0.15
0.10
0.05
ATc
- + - + - +
WT
rTgApiCox25
cTgApiCox25-HA/
rTgApiCox25
D
0.731
0.678
< 0.0001
0.004
1.00
Basal mOCR
(pmol / min / 1.5 x 10^6 parasites)
120
100
80
60
40
20
0
WT
rTgApiCox25
0 3 0 1 2 3
Days on ATc
E
Basal mOCR
(pmol / min / 1.5 x 10^6 parasites)
100
80
60
40
20
0
0 10 20 30 40 50
ECAR
(mpH / min / 1.5 x 10^6 parasites)
Days on ATc
0
1
2
3
rTgApiCox25
0
3
WT
0
WT + CHX

Figure 5 - figure supplement 1

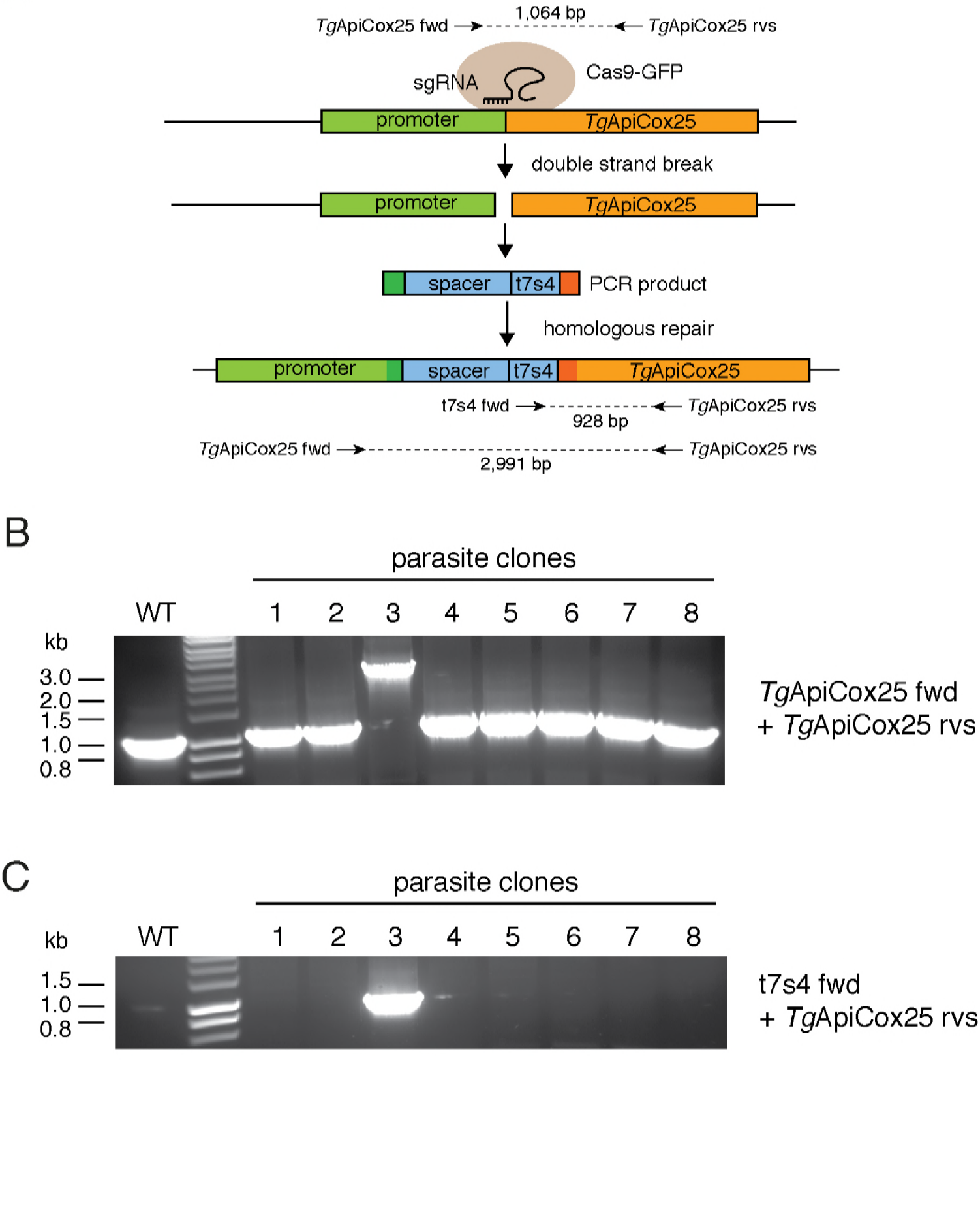

Figure 5 - figure supplement 2

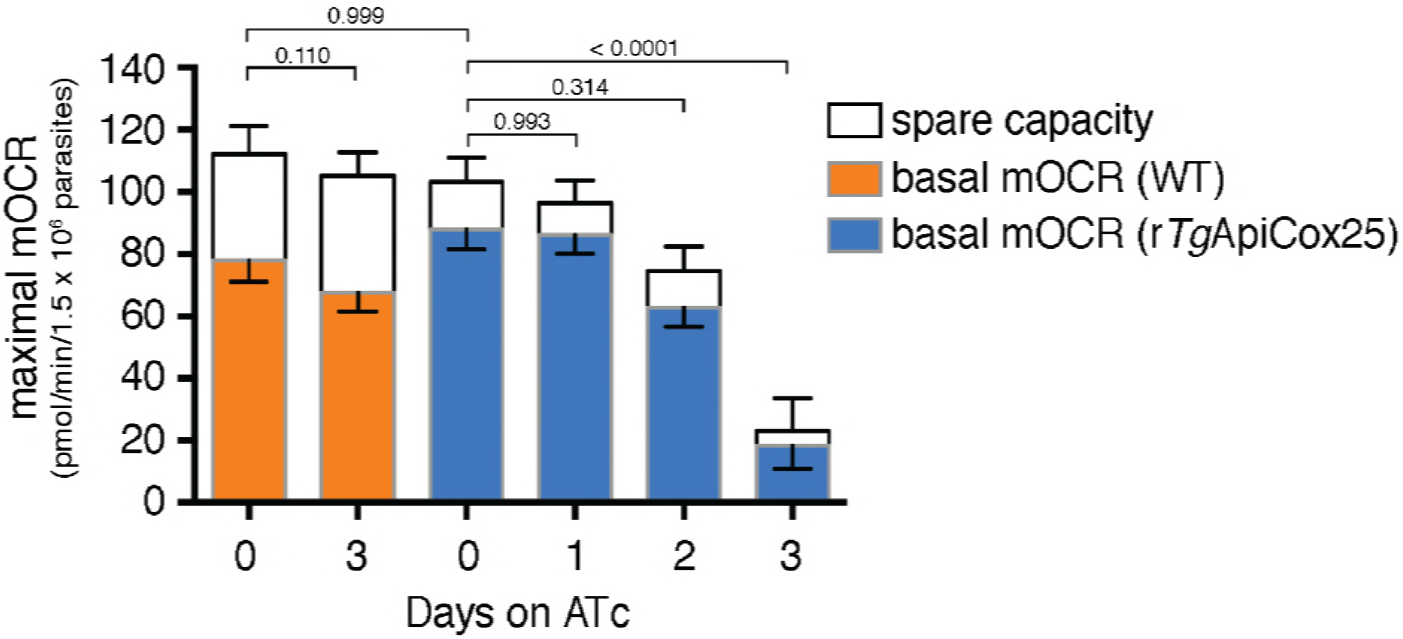

Figure 5 - figure supplement 3

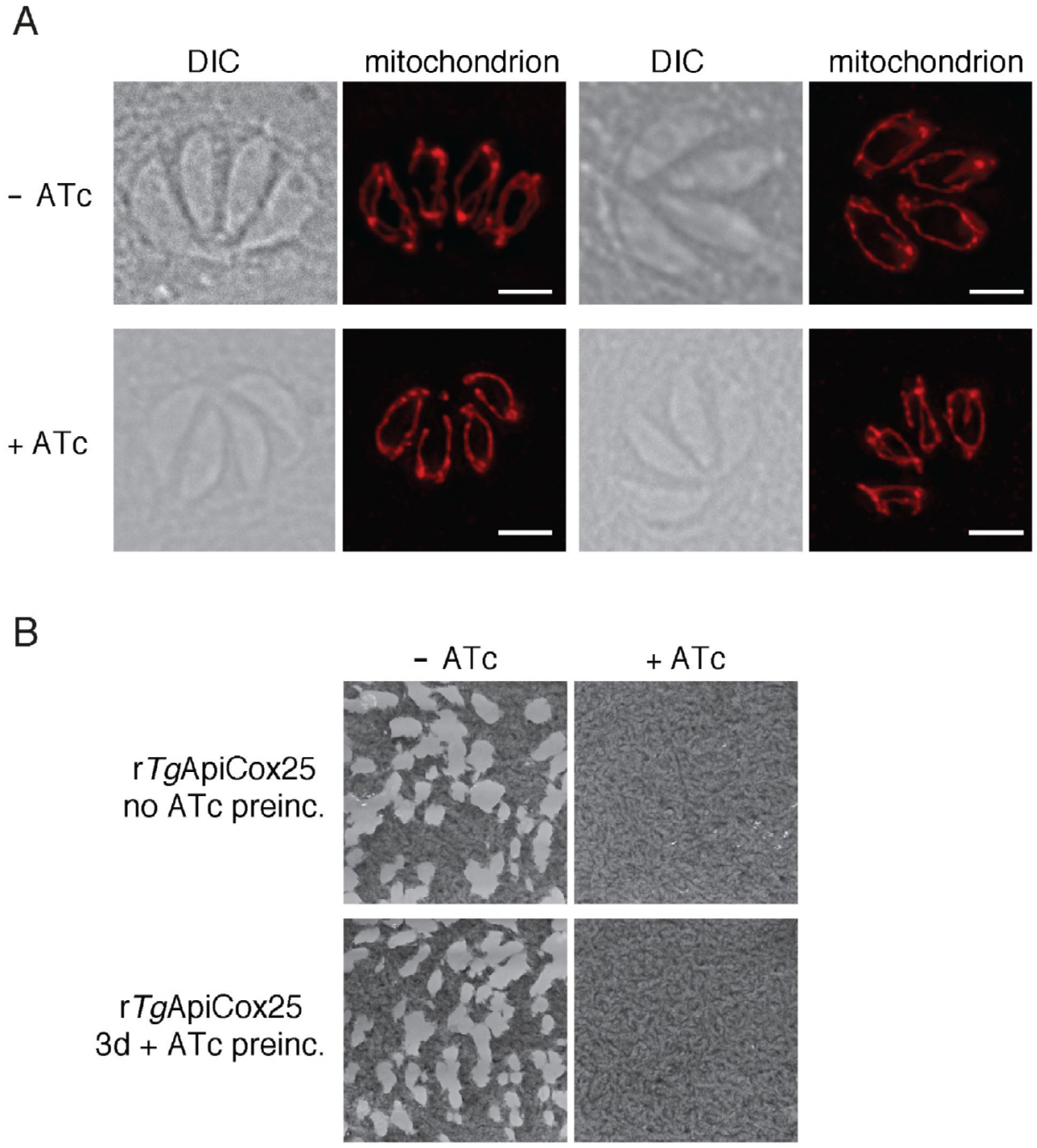

Figure 6

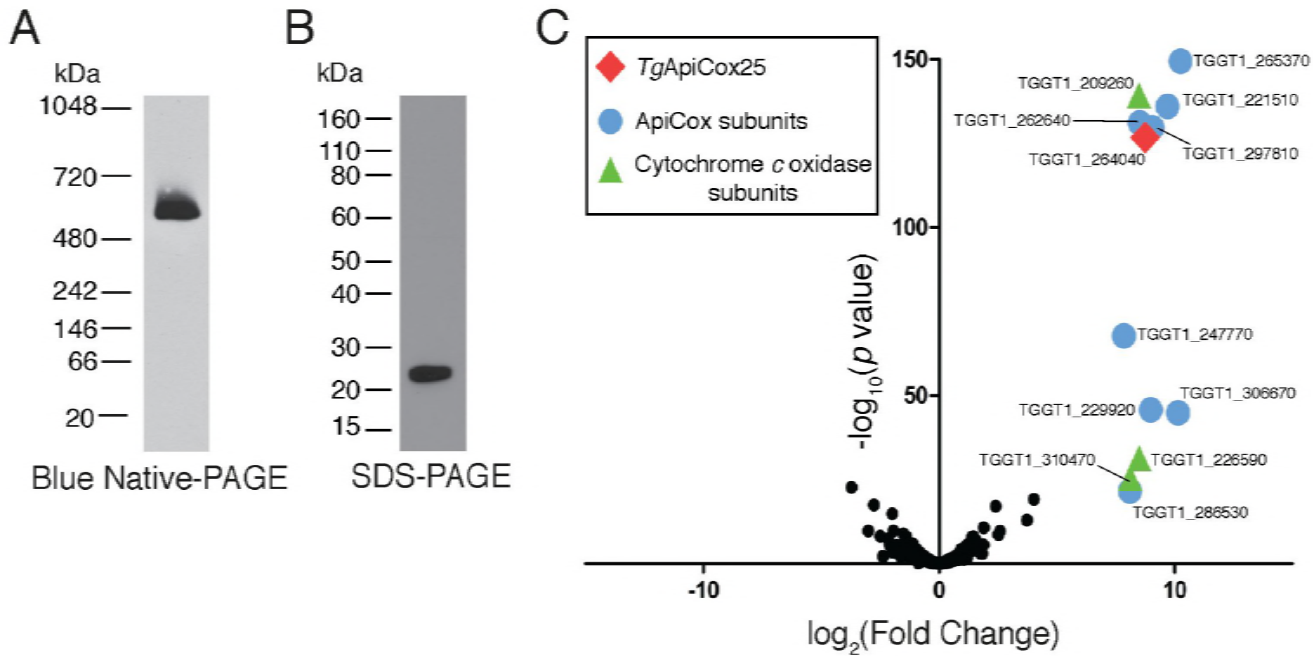
A
kDa
1048
720
480
242
146
66
20
Blue Native-PAGE
B
kDa
160
110
80
60
50
40
30
20
15
SDS-PAGE
C
TgApiCox25
ApiCox subunits
Cytochrome c oxidase subunits
150
100
50
-log10(p value)
TGGT1_265370
TGGT1_209260
TGGT1_221510
TGGT1_262640
TGGT1_264040
TGGT1_297810
TGGT1_247770
TGGT1_306670
TGGT1_229920
TGGT1_310470
TGGT1_226590
TGGT1_286530
-10
0
10
log2(Fold Change)

Figure 6 - figure supplement 1

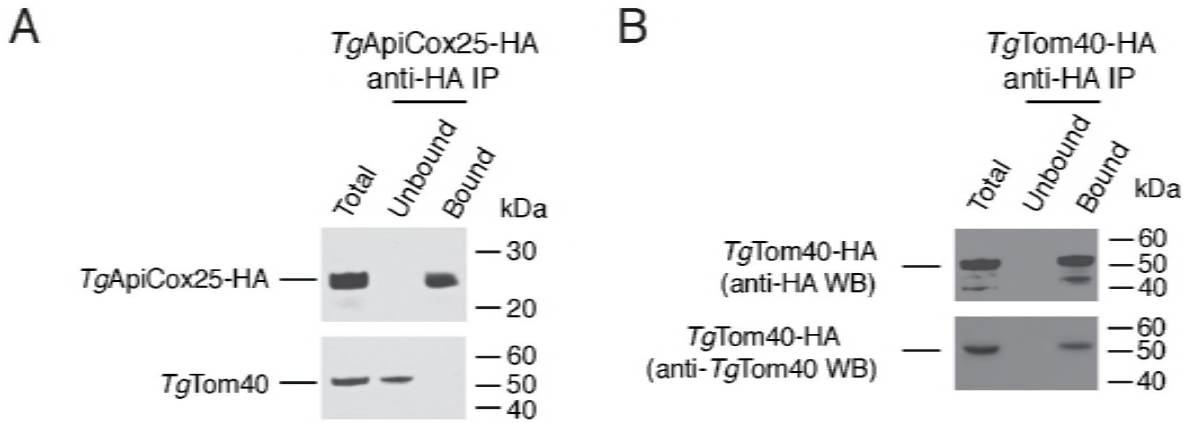

Figure 7

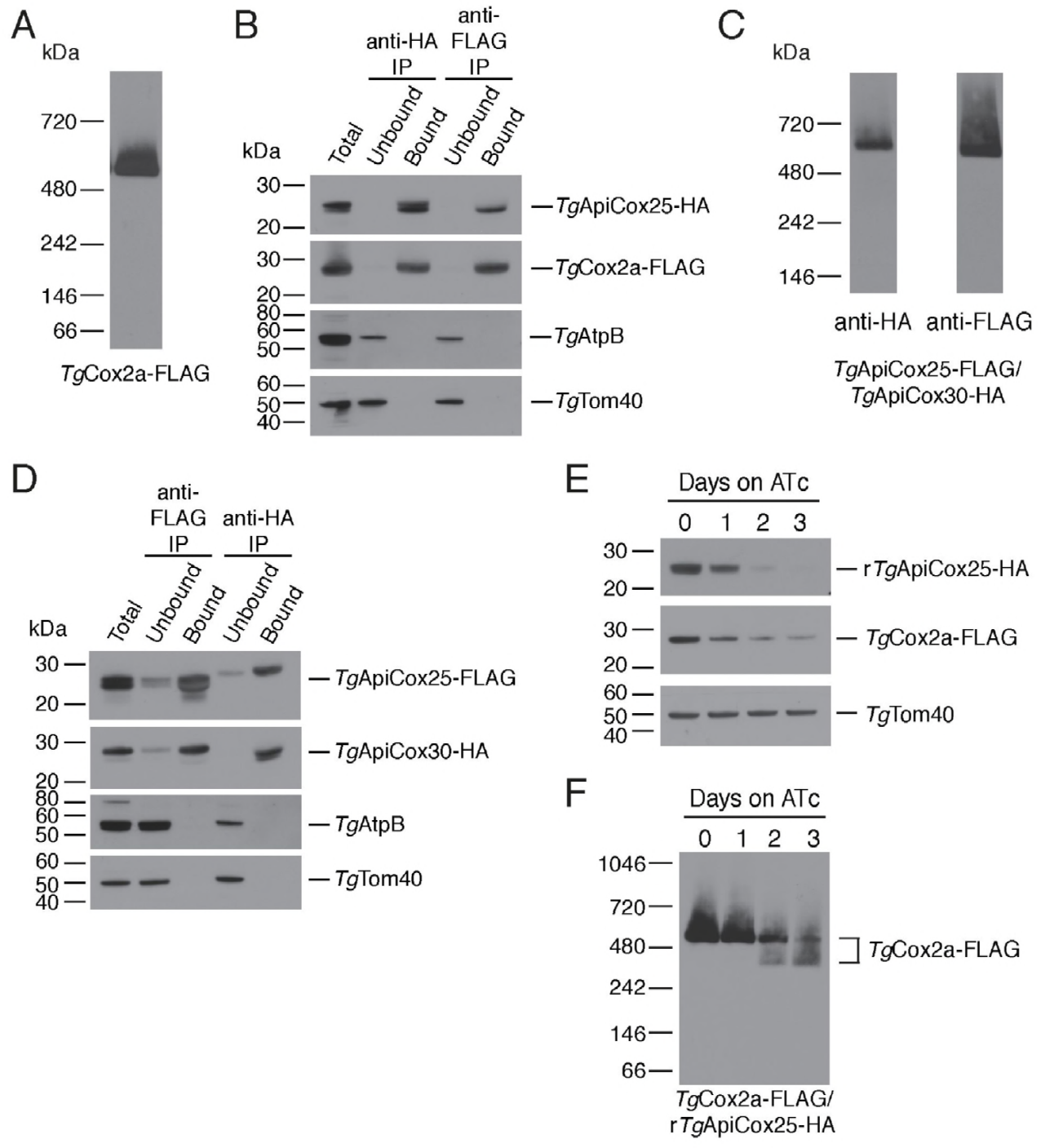
A
kDa
720
480
242
146
66
TgCox2a-FLAG
B
anti-HA IP
anti-FLAG IP
Total
Unbound
Bound
Unbound
Bound
kDa
30
20
TgApiCox25-HA
30
20
TgCox2a-FLAG
80
60
50
TgAtpB
60
50
40
TgTom40
C
kDa
720
480
242
146
anti-HA
anti-FLAG
TgApiCox25-FLAG/
TgApiCox30-HA
D
anti-FLAG IP
anti-HA IP
Total
Unbound
Bound
Unbound
Bound
kDa
30
20
TgApiCox25-FLAG
30
20
TgApiCox30-HA
80
60
50
TgAtpB
60
50
40
TgTom40
E
Days on ATc
0
1
2
3
30
20
rTgApiCox25-HA
30
20
TgCox2a-FLAG
60
50
40
TgTom40
F
Days on ATc
0
1
2
3
1046
720
480
242
146
66
TgCox2a-FLAG
TgCox2a-FLAG/
rTgApiCox25-HA

Figure 7 - figure supplement 1